2008

Wind tunnel study on the wake bubble of model trucks

Dongqing Yang
University of Windsor

WIND TUNNEL STUDY ON THE WAKE BUBBLE OF MODEL TRUCKS

By

Dongqing Yang

A Thesis

Submitted to the Faculty of Graduate Studies through the Department of Mechanical, Automotive and Materials Engineering in Partial Fulfillment of the Requirements for the Degree of Master of Applied Science at the University of Windsor

Windsor, Ontario, Canada

2008

Your file Votre référence
ISBN: 978-0-494-47019-0
Our file Notre référence
ISBN: 978-0-494-47019-0

Declaration of Co-Authorship/Previous Publication

I. Co-Authorship Declaration

I am aware of the University of Windsor Senate Policy on Authorship and I certify that I have properly acknowledged the contribution of other researchers to my thesis, and have obtained written permission from each of the co-author(s) to include the above material(s) in my thesis.

I certify that, with the above qualification, this thesis, and the research to which it refers, is the product of my own work.

II. Declaration of Previous Publication

This thesis includes one original paper that has been previously published for publication in peer reviewed conference, as follows:

Thesis Chapter	Publication title/full citation	Publication status*
Chapter 3, 4	Dongqing Yang, Shaohong Cheng, David S-K Ting, Wind Tunnel Study on the "Wake Bubble" of Model Truck, SAE Technical Series, 2008010739, 2008	Published

I certify that I have obtained a written permission from the copyright owner(s) to include the above published material(s) in my thesis. I certify that the above material describes work completed during my registration as graduate student at the University of Windsor.

I declare that, to the best of my knowledge, my thesis does not infringe upon anyone's copyright nor violate any proprietary rights and that any ideas, techniques, quotations, or any other material from the work of other people included in my thesis, published or otherwise, are fully acknowledged in accordance with the standard referencing practices. Furthermore, to the extent that I have included copyrighted material that surpasses the bounds of fair dealing within the meaning of the Canada Copyright Act, I certify that I have obtained a written permission from the copyright owner(s) to include such material(s) in my thesis.

I declare that this is a true copy of my thesis, including any final revisions, as approved by my thesis committee and the Graduate Studies office, and that this thesis has not been submitted for a higher degree to any other University of Institution.

Abstract

Heavy traffic volume makes tailgating a common picture on the road today. Wake interference, particularly in the scenario when a relatively small sedan drives into the wake of a large truck, may raise some serious highway safety concerns. In this study, the characteristics of separation bubble in the wake of model trucks with various degrees of model details are studied. The objective is to uncover the impact of truck model details on the characteristics of the wake bubble. Furthermore, how the spacing between the leading sedan and truck affects the bubble is also investigated. The hotwire measurements as well as flow visualization using a tuft grid have been conducted in a closed-loop wind tunnel at $Re=2-7\times10^5$. The wind tunnel results revealed that both the degree of model details and the spacing between sedan and truck have significant impact on the three dimensional structure of the wake bubble.

Acknowledgements

I would like to express my sincere thanks to Dr. Shaohong Cheng and Dr. David S-K Ting for their invaluable supervision, patience, encouragement and guidance throughout this research. Sincere gratitude is also expressed to my committee members: Dr. R. Carriveau and Dr. G. Rankin for their helpful comments, suggestions and their valuable time.

The technical support from Mr. Andrew Jenner and Mr. Patrick Seguin is much appreciated. I would also like to thank the staff in technical support center for their suggestions and helpful assistance. Special thanks to Ms. Yaoyao Zhang for her assistance during the flow visualization work.

I am also grateful to the research grants from the Natural Sciences and Engineering Research Council of Canada (NSERC) for this study.

Table of Contents

Declaration of Co-Authorship/Previous Publication iii

Abstract v

Acknowledgements vi

List of Tables x

List of Figures xi

List of Abbreviations, Symbols, Nomenclature xv

Chapter 1 Introduction ..... - 1 -

1.1 Background ..... - 1 -

1.2 Motivation ..... - 2 -

1.3 Objectives ..... - 4 -

Chapter 2 Literature Review ..... - 5 -

2.1 Wind Tunnel Testing ..... - 5 -

2.1.1 Ground Simulation ..... - 5 -

2.1.2 Flow Visualization ..... - 7 -

2.1.3 Reynolds Number Effect ..... - 8 -

2.2 Road Vehicle Model ..... - 12 -

2.3 Wake Structure of a Road Vehicle ..... - 14 -

2.4 Wake Investigation Using Hot-wire Anemometry ..... - 17 -

Chapter 3 Experimental Details ..... - 19 -

3.1 Test Setup ..... - 19 -

3.1.1 Wind Tunnel ..... - 19 -

3.1.2 Elevated Plate ..... - 19 -

3.2 Vehicle Models ..... - 22 -

3.2.1 Truck Model Design ..... - 22 -

3.2.2 Truck Models ..... - 24 -

3.2.3 Sedan Model ..... - 27 -

3.3 Hot-wire System ..... - 28 -

3.4 Flow Visualization Setup ..... - 30 -

Chapter 4 Results and Discussion ..... - 32 -

4.1 Shape Details Impact ..... - 32 -

4.2 Elevated Plate Impact ..... - 41 -

4.3 Three Dimensional Wake Bubble ..... - 45 -

4.4 Sedan and Truck in Tandem Arrangement ..... - 51 -

4.5 Reynolds Number Effect ..... - 53 -

4.6 Flow Visualization Using Tuft Grid ..... - 57 -

Chapter 5 Conclusions and Recommendations ..... - 61 -

References ..... - 64 -

Appendix A. Calculation of displacement thickness (wind tunnel board) ..... - 68 -

Appendix B. Uncertainty of a velocity sample ..... - 69 -

Appendix C. Sensitivity analysis ..... - 71 -

Appendix D. Traverse program (motion control of the traverse system) ..... - 77 -

Appendix E. Data collection program ..... - 80 -

Vita Auctoris ..... - 86 -

List of Tables

Table 2.1 Increasing the effective Re by screen application ..... - 11 -

Table 3.1 Comparison regarding elevated ground plate ..... - 21 -

Table 3.2 Relative surface roughness of the simplified truck models (rectangular block, rounded front model and generic model) ..... - 27 -

Table 4.1 Parameters in the first series of tests ..... - 34 -

Table 4.2 Recirculation length of the models at $Re=7\times10^5$ ..... - 38 -

Table 4.3 Parameters in the rest series of tests ..... - 41 -

Table 4.4 Recirculation length of the models ($Re=7\times10^5$, with/ without elevated plate) ..... - 45 -

Table 4.5Detection of bubble for different truck models ..... - 50 -

Table 4.6 Detection of bubble on the real shape model ..... - 52 -

Table 4.7 Extrapolating the results (recirculation length of real shape model) ..... - 54 -

Table 4.8 Comparison of recirculation length of the models between two techniques (hotwire vs. tuft grid, under $Re=7\times10^5$, with elevated plate) ..... - 59 -

List of Figures

Figure 2.1 Ways for representing the road in a wind tunnel [Hucho, 1993] ..... - 7 -

Figure 2.2 Trailing vortices in the wake of a car [JSME, 1988] ..... - 8 -

Figure 2.3 Setup of road vehicle in the open test section [Wiedemann, 1989] ..... - 9 -

Figure 2.4 Pressure distribution on a road vehicle at different Re: no screen [Wiedemann, 1989] ..... - 10 -

Figure 2.5 Pressure distribution on a road vehicle at different Re: Turbulence modified by a screen [Wiedemann, 1989] ..... - 10 -

Figure 2.6 Drag coefficient of a road vehicle without ground plane vs. Re [Wiedemann, 1989] ..... - 11 -

Figure 2.7 Bluff bodies used for vehicle modeling [Allan,1981] ..... - 12 -

Figure 2.8 Ahmed body [Ahmed et al, 1984] ..... - 13 -

Figure 2.9 Sample of truck model [McCallen, 1999] ..... - 14 -

Figure 2.10 Effect of slanting the blunt base of 3D bodies on drag coefficients [Losito & Nicola, 1983] ..... - 15 -

Figure 2.11 Horse shoe vortex system in the near wake region of an Ahmed body ..... - 16 -

Figure 2.12 Schematic view of the road vehicle model and bubble length at two successive time [Duell & George, 1999] ..... - 17 -

Figure 3. 1 Wind tunnel ..... - 19 -

Figure 3.2 Application of elevated plate (not to scale) ..... - 20 -

Figure 3.3 Velocity profiles at 5 stations downstream of the elevated plate leading edge and measured boundary layer along the plate ..... - 22 -

Figure 3.4 Rounded front model Current study (solid line) vs. Duell & George's work (dash line) [1999] ..... - 23 -

Figure 3.5 Three view drawings and the real picture of the rectangular block .... - 24 -

Figure 3.6 Three view drawings and the real picture of the rounded front model ..... - 25 -

Figure 3.7 Side and front views and the real picture of the generic model ..... - 26 -

Figure 3.8 Side and front views of scaled specific model ..... - 26 -

Figure 3.9 Side and front view of sedan model ..... - 28 -

Figure 3.10 Hot-wire system [CTA: Dantec Streamline 55C90, I/O: shielded I/O connector block for DAQ devices, A/D: PCI-6071E] ..... - 28 -

Figure 3.11 Experimental arrangement for smoke visualization ..... - 31 -

Figure 3.12 Experimental arrangement for tuft visualization ..... - 31 -

Figure 4.1 Experimental arrangement for studying wake of the truck model: single truck-vertical central plane without elevated plate ..... - 32 -

Figure 4.2 Grid for data collection ..... - 33 -

Figure 4.3 Wake centerlines ..... - 35 -

Figure 4.4 Near wake time averaged velocity distribution at the vertical central plane and recirculation length ..... - 35 -

Figure 4. 5 Bubble shape of the rectangular block and corresponding mean velocity contour in the wake at Re=7×10^5 ..... - 36 -

Figure 4. 6 Bubble shape of the rounded front model and corresponding mean velocity contour in the wake at Re=7×10^5 ..... - 36 -

Figure 4. 7 Bubble shape of the generic model and corresponding mean velocity contour in the wake at Re=7×10^5 ..... - 37 -

Figure 4. 8 Bubble shape of the real truck model and corresponding mean velocity contour in the wake at Re=7×10^5 ..... - 37 -

Figure 4. 9 Streamwise velocity distribution at the horizontal line where recirculation length can be determined ..... - 38 -

Figure 4. 10 Comparison of bubble shapes of all the truck models ..... - 39 -

Figure 4. 11 Smoke visualization of wake flow behind a real shape truck model. - 41 -

Figure 4. 12 Different ground simulations ..... - 42 -

Figure 4. 13 Bubble shape of the rectangular block ..... - 43 -

Figure 4. 14 Experimental arrangement for studying wake of the truck model: single truck case-vertical side planes ..... - 46 -

Figure 4. 15 Back view of vehicle model ..... - 46 -

Figure 4. 16 Three dimensional bubble of rectangular block ..... - 47 -

Figure 4. 17 Experimental arrangement for studying wake of the truck model: sedan and truck in tandem case ..... - 51 -

Figure 4. 18 Three dimensional bubble of real shape model: ..... - 52 -

Figure 4. 19 Application of perforated plate ..... - 53 -

Figure 4. 20 Bubble shape under different Re,"smooth flow" ..... - 55 -

Figure 4. 21 Bbubble shape under different Re,"turbulent flow" ..... - 55 -

Figure 4. 22 Recirculation length vs. Reynolds number (real shape model) ..... - 56 -

Figure 4. 23 Tuft visualization: U=4.2m/s (left) and U=8.2m/s (right) ..... - 57 -

Figure 4. 24 Tuft visualization: U=11.5m/s (left) and U=14.7m/s (right) ..... - 58 -

Figure 4. 25 Tuft visualization: U=4.2m/s (left) and U=8.2m/s (right) ..... - 58 -

Figure 4. 26 Tuft visualization: U=11.5m/s (left) and U=14.7m/s (right) ..... - 58 -

Figure 4. 27 Tuft visualization: X=0.5H downstream, 14m/s freestream ..... - 59 -

Figure 4. 28 Tuft visualization: X=H downstream, 14m/s freestream ..... - 60 -

Figure 4.29 Tuft visualization: X=1.5H downstream, 14m/s freestream ..... - 60 -

List of Abbreviations, Symbols, Nomenclature

Acronyms

A/D	Analogue/Digital
CTA	Constant Temperature Anemometer
DAQ	Data Acquisition
GM	Generic Model
HWA	Hot Wire Anemometry
I/O	Input/Output
RB	Rectangular Block model
RF	Rounded Front model
RS	Real Shape model
2-D	Two-dimensional
3-D	Three-dimensional

English symbols

C_d	Drag coefficient
C_p	Pressure coefficient
e/D	Relative roughness
H	Height of the model (m)
L	Length of the model (m)

Re	Reynolds number=VL/ υ
Tu	Turbulent intensity (%)
U_m	Local mean velocity (m/s)
U_∞	Free stream velocity (m/s)
V	Velocity (m/s)
W	Width of the model (m)
X	Distance between model base and downstream Point (m)

Greek symbols

υ	Kinematic viscosity of air (m^2/s)
Ψ	Slant angle (°)
Ψ_c	Critical slant angle (°)

Chapter 1 Introduction

1.1 Background

Rarely are vehicles on the road alone. They typically pass or follow each other in close proximity, whether on the highway or on a racing track. The flow field of each vehicle is thus influenced by the presence of the other vehicles; in other words, the flow fields interact with each other [Hucho, 1998]. Large road vehicles generate relatively large wakes, the characteristics of which are worth studying as far as highway safety is concerned. In spite of many years of progress, our understanding on the flow characteristics in the near wake of the tractor-trailer shape vehicle, a common vehicle type on the road in North America, is still very immature.

Wind tunnel and road tests have long been used for the analysis and assessment of aerodynamic performance of road vehicles. Furthermore, progressively advanced numerical models also gain ground in road vehicle performance study [Sinisa, 2002; Sitlani & Aung, 2006]. Nevertheless, due to the challenges in accurately simulating complicated flow around a detailed vehicle, and the high cost involved in road vehicle testing, wind tunnel tests still play an important key role in road vehicle research.

1.2 Motivation

To better understand the fluid mechanics which affects vehicle fuel consumption, vehicle safety, and passenger comfort, it is necessary to study the time dependent near wake flow field behind ground vehicle bodies [Duell & George, 1999]. As far as vehicle aerodynamics is concerned, drag is always the focus of the research work, for a reduction in drag would lead to a reduction in fuel consumption. In general, there are two main kinds of drag a vehicle encounters on the road: the pressure drag and the friction drag. The drag of a road vehicle is primarily caused by the pressure deficit in the wake. Thus, among the flow fields of a road vehicle, the flow region in the near wake plays a key role on the aerodynamic performance of a road vehicle.

Many research works have been done to understand how flow around a vehicle affects its driving stability and drag [Allen, 1981& Ahmed, 1984]. Aerodynamic interaction between multiple bluff bodies, such as two cubes of the same geometrical size [Martinuzzi & Havel, 2004], has been extensively studied due to its practical significance in many engineering applications. Till now, the relevant works in studying the aerodynamic interference between vehicles of different sizes were mainly based on pressure measurement [Azim, 1994] and force measurement [Hammache et al, 2001]. Information obtained from detailed velocity

measurement is expected to complement these studies, significantly advancing present knowledge on road vehicle aerodynamics.

Moreover, the knowledge of how the details of vehicle shape affect the aerodynamic performance is still lacking, and how much shape detail is needed to maintain the real aerodynamic characteristics is also worth studying.

In short, a better understanding of wake bubble of the road vehicle is necessary, be it a single one or following other vehicles, since the low-frequency oscillation inside the vehicle wake bubble can affect the stability of the driver-vehicle combination. Furthermore, once the relation between the wake bubble and the drag is uncovered, a better understanding of drag manipulation can be realized.

1.3 Objectives

1) For the single truck model measurement:

   - Obtain the bubble length in the near wake of four truck models with various levels of model details;
   - By comparing the results, find out how the shape details affect the near wake of truck models;
   - Find out the impact of application of elevated plate on the characteristic of the wake bubble.
   - Extend the measurement to the side vertical planes to investigate the 3D bubble feature.

2) For the sedan and truck in tandem arrangement (sedan in the front):

   Conduct the hotwire measurement behind the truck model in order to find out the impact of spacing of sedan and truck model on the wake structure.

3) Study the Reynolds number effect

Chapter 2 Literature Review

2.1 Wind Tunnel Testing

The advantage of wind tunnel test is that data can be obtained on models (even in reduced scale) in a very early development phase, which allows an estimate of the dynamics of a vehicle concept long before drivable prototype is available.

However, wind tunnel tests cannot perfectly simulate the on road conditions [Hucho, 1998]. The main limitations are:

i) The relative motion between vehicle and road is hardly reproduced; the floor should move with wind.

ii) On the road, a vehicle moves through a space of infinite dimensions ("free air"). In contrast, the dimensions of a wind tunnel test section are limited and comparatively small.

iii) Reynolds number which represents the real life scenario can hardly be reached.

2.1.1 Ground Simulation

Probably one of the most ideal ways to determine the aerodynamics of a vehicle would be to mount a model on a catapult carriage with a zipper slot similar to an aircraft catapult. The catapult should be several miles long and housed in a closed

building with a cross-sectional area at least several hundred times the model frontal area. This idea, while not impossible, is however, not economically practical [D. S. Gross et al, 1966]. In general, there are several ways to achieve the on road simulation. The simplest and conventional way is with a solid and fixed ground floor [Figure 2.1, a]. The drawback is that it may have considerable boundary layer effect; an improved method is raised, an elevated plate is applied so as to reduce the boundary layer effect [Figure 2.1, e], the length of the elevated plate required depends on the models to be tested but is commonly made the length of test section. The typical height will be three to five times the thickness of the floor boundary layer [Barlow et al, 1999]. A new and therefore thinner boundary layer begins along the plate; there is also mirror image method [Figure 2.1, b], model costs have to be doubled, moreover, the flow is not necessarily symmetrical. The moving belt [Figure 2.1, c] seems to represent a perfect approach as mentioned, despite lots of issues needed to be addressed properly: is the belt strong enough to support the weight of the model, how to synchronize the moving speed of the belt etc. There are other approaches dealing with boundary layer effect as well, such as boundary layer suction [Figure 2.1, d &g] and lift model above the boundary layer [Figure 2.1, f].

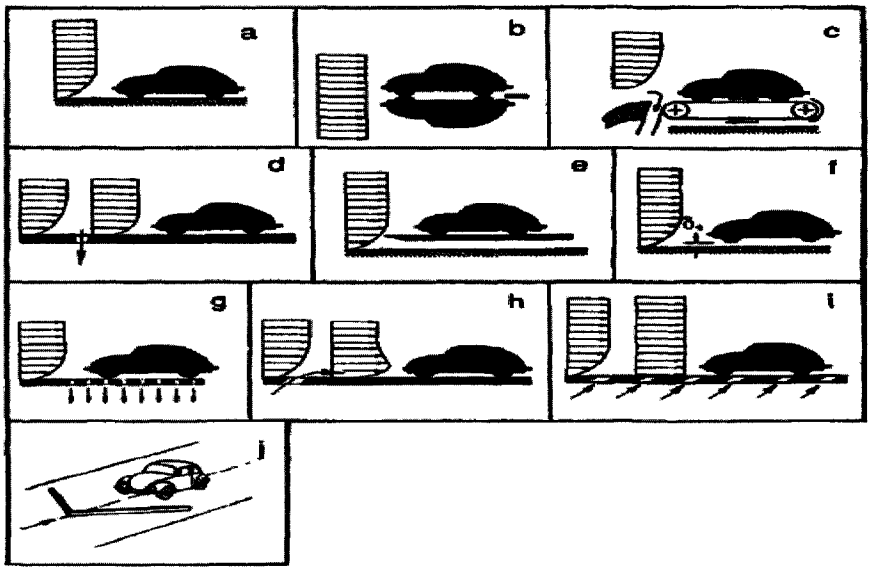

Figure 2. 1 Ways for representing the road in a wind tunnel [Hucho, 1993]

2.1.2 Flow Visualization

Flow visualization is an extremely powerful experimental technique for gaining insight into the fluid flow [Granger, 1985]. A variety of flow visualization methods have been applied in vehicle aerodynamic field, such as smoke, tufts etc.

Smoke is the conventional way for flow visualization. By blowing smoke into an airstream, the course of airflow becomes visible. However, smoke cannot be used in recirculating flows. The smoke also tends to obscure parts of a three-dimensional model, so it is most often used to visualize two-dimensional models in narrow tunnels. Furthermore, smoke is awkward to handle.

Tufts (usually wool, tufted nylon, or cotton) are often used to discover the direction of the flow. They are often used to identify the region of the wake, separation line, instability and transition, see Figure 2.2. Normally it works best in a range of 1m/s

up to 30m/s. If the tufts are in a wake, they will flutter around and point in random directions, often into the incoming free air stream [Smith, 1992].

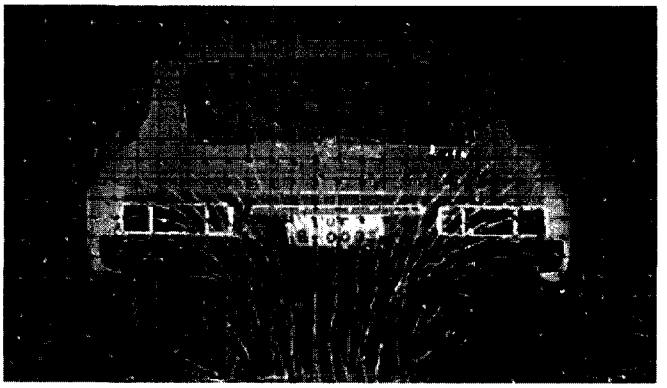

Figure 2. 2 Trailing vortices in the wake of a car [JSME, 1988]

2.1.3 Reynolds Number Effect

The scaling problem is frequently encountered in the aerodynamic research field since most wind tunnels are not big enough to accommodate full scale vehicles. The results from scaled model may be very misleading since the kinematic similarity can not be met. On the other hand, due to the high cost and uncontrollable environmental conditions, there are rare cases in which a full scale vehicle can be ground tested to operational speed. So methods of extrapolation are very important [Barlow et al, 1999].

In other words, the advantage of working with reduced-scale models are realized only if the results achieved with them can reliably be transferred to full scale. There are generally two paths leading to this target: Reynold' s law has to be strictly observed or by making use of other effects, a higher Re can be simulated. In road

vehicle testing, it is fairly difficult to maintain the desired Re when scaled model is used, even the top speed is satisfied, the Mach number effects become noticeable at relatively low wind speed [Hucho, 1998].

In 1989, Wiedemann proved that for a complex configuration like road vehicle, it is effective to manipulate the turbulence of the oncoming flow in order to decrease the "effective" Re (For sphere, it was already proved by Dryden in 1936). More specifically, when a screen of adequate mesh and bar size in the wind tunnel inlet is used, pressure distribution corresponding to different Reynolds numbers nearly fall onto a single curve that is equivalent to an increase of the effective Reynolds number, see Figure 2.3-2.5 for details.

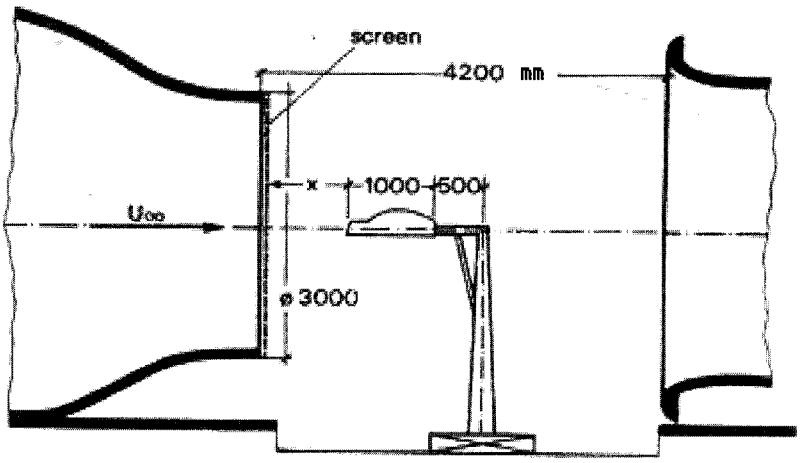

Figure 2. 3 Setup of road vehicle in the open test section [Wiedemann, 1989]

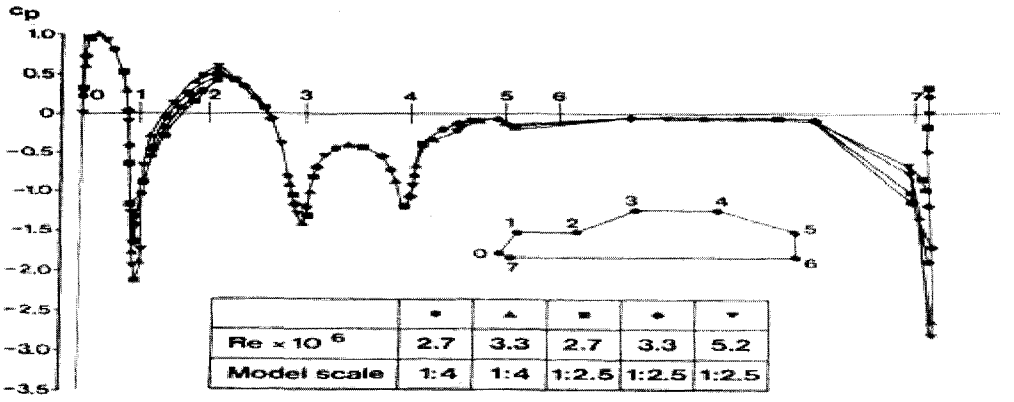

Figure 2. 4 Pressure distribution on a road vehicle at different Re: no screen [Wiedemann, 1989]

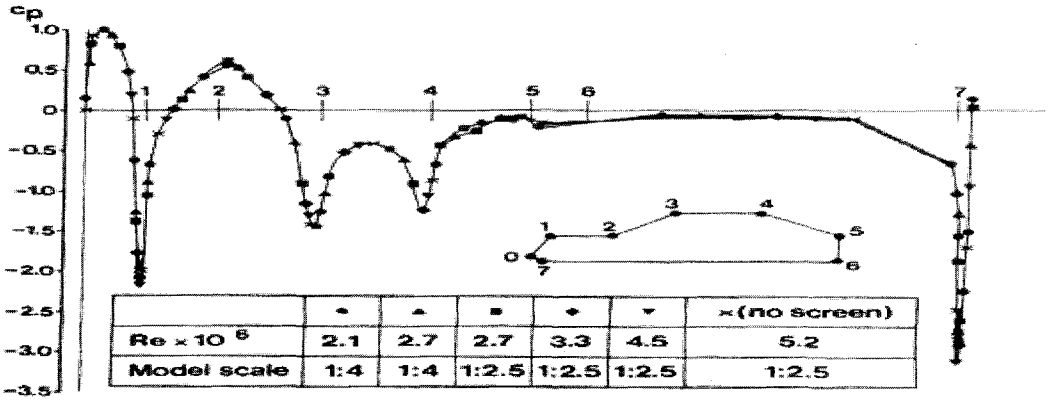

Figure 2. 5 Pressure distribution on a road vehicle at different Re: Turbulence modified by a screen [Wiedemann, 1989]

There is a strong dependence of the pressure coefficient C_p on the Re, as can be seen in Figure 2.4. Figure 2.5 shows the pressure distribution for the same range of Re but with a screen mounted at the inlet. This time the results nearly fall onto a single line, which means there is no significant Re effect on pressure distribution if screen is applied. Moreover, it shows that the results of $Re=5.2\times10^6$ without screen case and $Re=2.7\times10^6$ with screen case are almost identical.

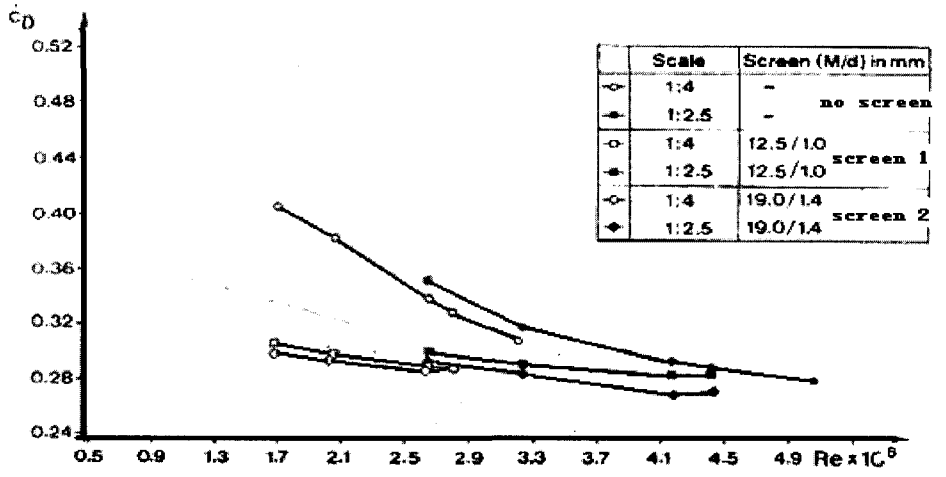

Figure 2.6 Drag coefficient of a road vehicle without ground plane vs. Re

[Wiedemann, 1989]

For the drag coefficient measurement, see Figure 2.6, both screen 1 and 2 lead to a considerable decrease of drag, the clean flow needs about $Re=3.8\times10^6$ to yield $C_d=0.3$, using screen 1 for example, this can be achieved by $Re=2.5\times10^6$. This is equivalent to increase of the effective Re by a factor of 3.8/2.5=1.52.

Table 2.0.1 Increasing the effective Re by screen application

Screen mounted at the wind inlet	Increase the effective Re by a factor of [Pressure distribution on the model vehicle]	Increase the effective Re by a factor of [Drag coefficient]
Screen 1	1.93*	1.52
Screen 2	1.93	1.73

Note: the result at $Re=2.7\times10^6$ with screen is equivalent to the result at $Re=5.2\times10^6$

without screen mounted at the wind tunnel inlet. Thus the effective Re can be increased by a factor of $5.2\times10^6/2.7\times10^6=1.93$.

2.2 Road Vehicle Model

In vehicle aerodynamics, ground vehicles can always be termed as bluff bodies moving in close vicinity of the road surface. In the simplest case, a rectangular block can be used to model a road vehicle. Figure 2.7 shows some simple bluff bodies used by Allan [1981] when studying the flow field around the tractor-trailer type vehicle.

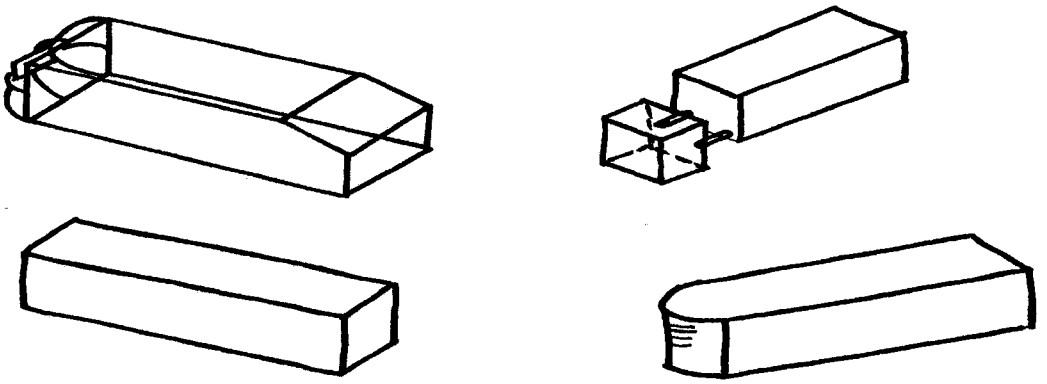

Figure 2.7 Bluff bodies used for vehicle modeling [Allan,1981]

The main problem with simplified bluff shapes is that they may not accurately reflect the complex aerodynamic shape of vehicles. In order to obtain the essential features of the flow field around a real vehicle, Ahmed body [Ahmed et al, 1984], as illustrated in Figure 2.8, was developed for studying aerodynamics of passenger vehicles. Ahmed body is a simple model which can provide the strong

three-dimensional flow in the front, relative uniform flow in the middle and large structured wake at the rear of a real passenger car, without worrying about the unique features associated with different vehicle models.

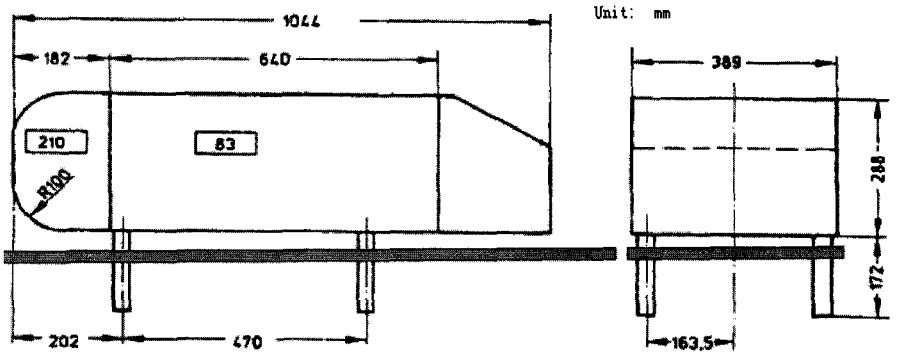

Figure 2.8 Ahmed body [Ahmed et al, 1984]

For the relative large tractor trailer type vehicles, the modeling is somewhat different compared with that of passenger vehicles. Specifically, trucks have no slant angle at the rear end and the overall geometry is longer (larger). To the best of our knowledge, there is no classical or typical (Ahmed) truck model available in the vehicle aerodynamics field. One of the main concerns of research on truck is the effect of the tractor-trailer gap on the overall drag [McCallen, 1999]. As can be seen in Figure 2.9, the gap of the truck model is adjustable. Some researchers have also considered the height mismatch between tractor and trailer as a parameter for drag reduction.

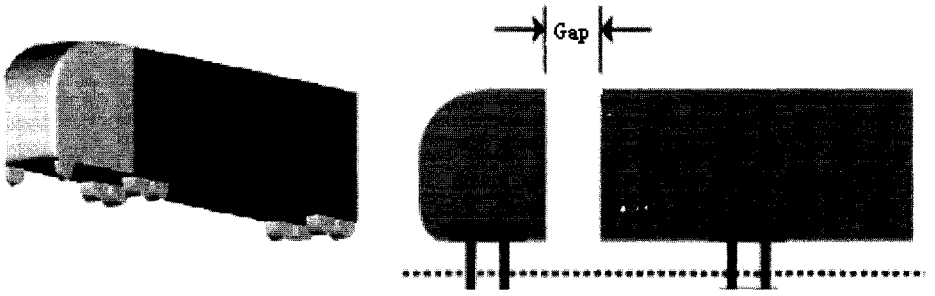

Figure 2.9 Sample of truck model [McCallen, 1999]

2.3 Wake Structure of A Road Vehicle

Based on flow visualization and interpretation of the aerodynamic force measurements, vehicle wake can be classified into four categories depending on the rear slant angle Ψ [Losito & Nicola, 1983], see Figure 2.10 for details.

1. Ψ=90° (square back type): Axisymmetric wakes with well organized bubble flows in the near wake .

2. $\Psi_C \leq \Psi \leq 90°$ (where Ψ_C is the critical angle): Three-dimensional wakes without embedded vortices.

3. $\Psi < \Psi_C$: Three-dimensional wakes with strong embedded longitudinal vortices.

4. $0 < \Psi < \Psi_C$: Three-dimensional wakes with weak vortices.

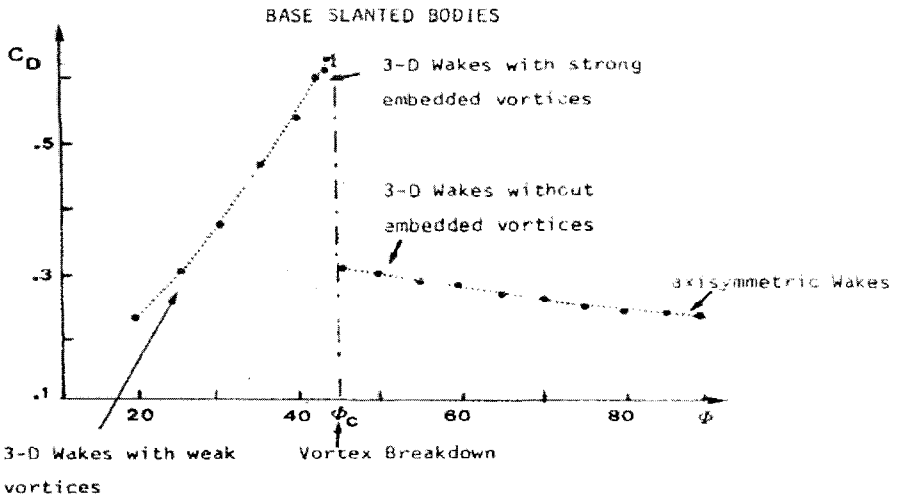

Figure 2. 10 Effect of slanting the blunt base of 3D bodies on drag coefficients [Losito & Nicola, 1983]

According to case 1 listed above, in the near wake region of a tractor trailer, well established large bubbles with a recirculating flow is evident.

The total drag of a car consists primarily of pressure drag [Hucho, 1998]. This is even more so for a truck as it is significantly less streamlined as compared to a passenger car. To reduce drag, the study of three-dimensional flow over ground vehicle has become a subject of significant importance in the automobile industry. Among the flow field around a vehicle, wake is the dominant part of the overall aerodynamics of a vehicle. Generally speaking, the complete wake consists of a near wake region and a far wake region separated by a shear layer which grows from the boundary layer at the separation point. The near wake of a ground vehicle

is a very complex separation region characterized by shear layers, unsteadiness, recirculation and streamwise vorticity.

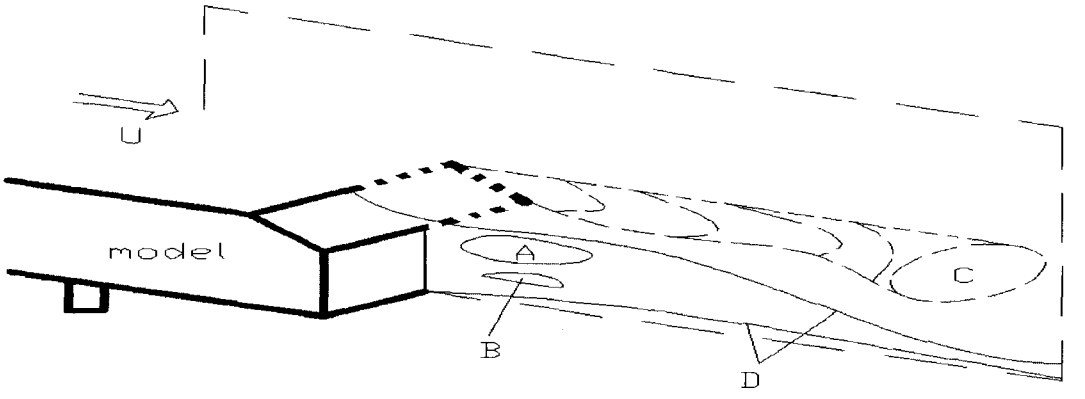

Figure 2.11 Horse shoe vortex system in the near wake region of an Ahmed body

Figure 2.11 illustrates the near wake region of a typical Ahmed body: "A" and "B" are the two recirculatory regions; "C" is the longitudinal vortex, the "separation bubble" is indicated by "D". Both "A" and "C" depend mainly on the slant angle while "B" depends primarily on the ground clearance gap [Ahmed et al, 1984]. For a model without slant angle, which is the case considered in this study, the vortex "C" hardly occurs.

An important characteristic of the near wake recirculation region is the recirculation length, X_r. It is defined as the distance between the model base and the mean location of the free stagnation point, as depicted in Figure 2.12. The location of the time-averaged free stagnation point can be deduced from the minimum of U_m/U_∞, (where U_m is the local mean velocity and U_∞ is the free stream velocity) or, the maximum of the root mean square fluctuating velocity intensity.

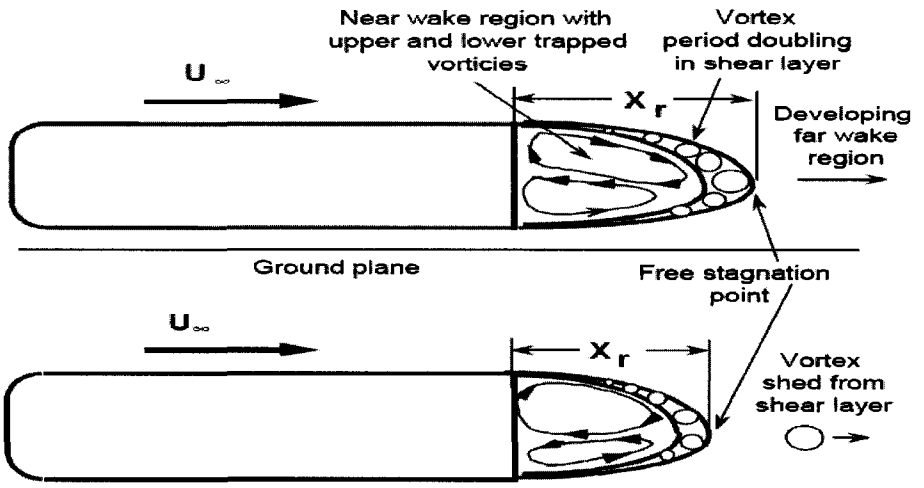

Figure 2. 12 Schematic view of the road vehicle model and bubble length at two successive time [Duell & George, 1999]

The free stagnation point of a separated flow is a quasi-periodically fluctuating point that shifts as vortices are shed from the shear layer that bounds the recirculation region [Duell & George, 1999], see Figure 2.12. The near wake velocity distribution is worth measuring since it determines the near wake size and locates the free stagnation point.

2.4 Wake Investigation Using Hot-wire Anemometry

A conventional way to consider a complex flow is to present the time averaged velocity field and the distribution of turbulence quantities obtained from a large number of single point measurement [Bearman, 1997]. LDA and PIV are not suitable for characterizing the time dependant fluid dynamics of wake due to low rate of data capture when air is the working fluid [Shaw et al, 2001].

It is generally recognized that hot wire anemometry is not ideal for velocity measurements in recirculating flows for two reasons: first, this technique can only measure the velocity magnitude normal to the hotwire but not associated flow directions. Also, the measured value of the local mean velocity becomes less accurate in highly turbulent flow fields. However, the velocity distribution obtained can still indicate the recirculation region. Measuring the near wake velocity distribution is important because it indicates the size of the near wake and can show any fundamental changes that have occurred to the near wake [Duell & George, 1993].

Chapter 3 Experimental Details

3.1 Test Setup

3.1.1 Wind Tunnel

In the present study, the experiments were conducted in a closed-loop wind tunnel as shown in Figure 3.1. The wooden-ground, steely-top test section of the wind tunnel has an overall dimension of 4m (Length) X 0.76m (Width) X 0.76m (Height). The free stream flow at the wind tunnel inlet is relatively smooth (T_u=0.5%) and the maximum obtainable velocity is around 20m/s.

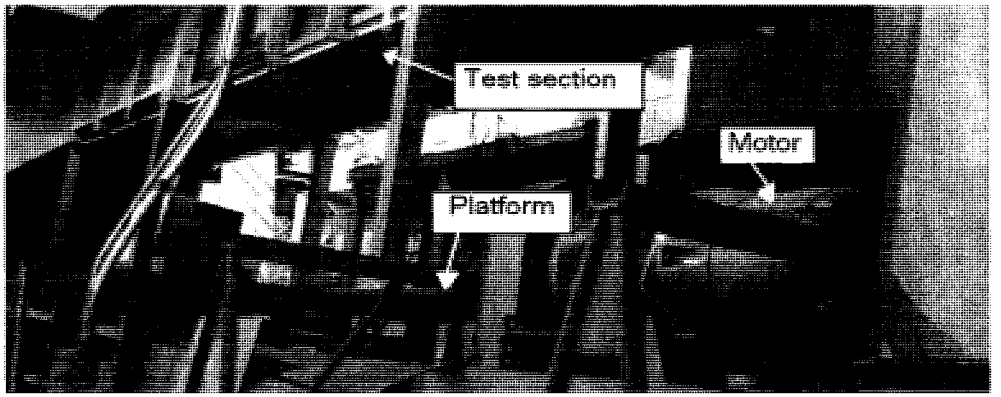

Figure 3. 1 Wind tunnel

3.1.2 Elevated Plate

According to Garni [2003], a fixed tunnel board is adequate for the study of ground vehicle as long as the displacement thickness of the ground boundary layer measured in the empty test section is less than 10% of the vehicle's ground

clearance. Current displacement thickness of the boundary layer at the location of rear truck corresponds to 6% of the vehicle model ground clearance. Therefore, the effect of the fixed tunnel board is expected to be small. See Appendix A for details. Nevertheless, an elevated ground board is fairly often used, mainly when a large wind tunnel is used for small-scale experiments [Hucho, 1998], since at the leading edge, a new boundary layer starts growing, but at zero thickness which results in a better boundary layer condition.

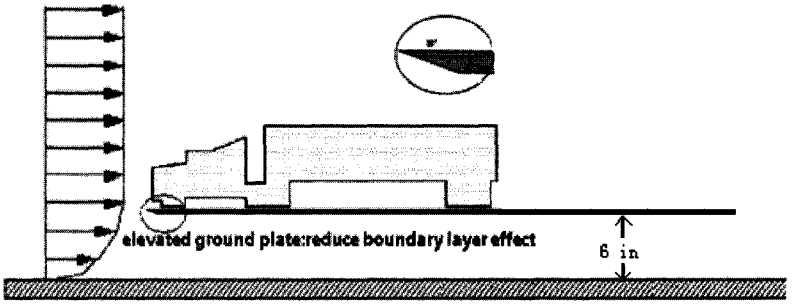

Figure 3.2 Application of elevated plate (not to scale)

The elevated plate is made of wood, it has a painted smooth surface, and the leading edge is sharpened as can be seen in Figure 3.2 in order to minimize the up wash flow. The overall geometry of the elevated plate is 1.52m (L) ×0.73m (W) × 0.02m (H). The length of the plate is twice the length of truck model; full span is used: the width of the plate is 0.03m (1 inch) less than the width of the tunnel for the sake of easy installation; the thickness of the plate is set to minimize possible vibration.

Barlow [1999] suggested that the clearance of the plate should be three to five times the thickness of the floor boundary layer. The measured floor boundary layer thickness is 0.04m (1.5 in) at the location of rear truck. So the clearance should fall in between 0.11-0.20m (4.5-7.5 in). The ground clearance of elevated plate is finally set to be 0.15m (6 in) after several trials of boundary layer thickness measurement.

Table 3.1 shows the comparison of current work with Garry's work [1991] regarding the elevated ground plate. The overall dimensions are quite close. Figure 3.3 illustrates the boundary layer growth along the elevated plate measured by hotwire system. The dimensionless distance X/L has been used, where X is the distance from the leading edge and L is the length of the elevated plate.

Table 3.0.1 Comparison regarding elevated ground plate

	Test section m×m (in×in)	Thickness of the plate m(in)	Clearance of the plate m(in)	span
Current study	0.76×0.76 (30×30)	0.02 (0.75)	0.15 (6)	full
Garry, 1991	0.91×0.91 (36×36)	0.02 (0.87)	0.18 (6.89)	full

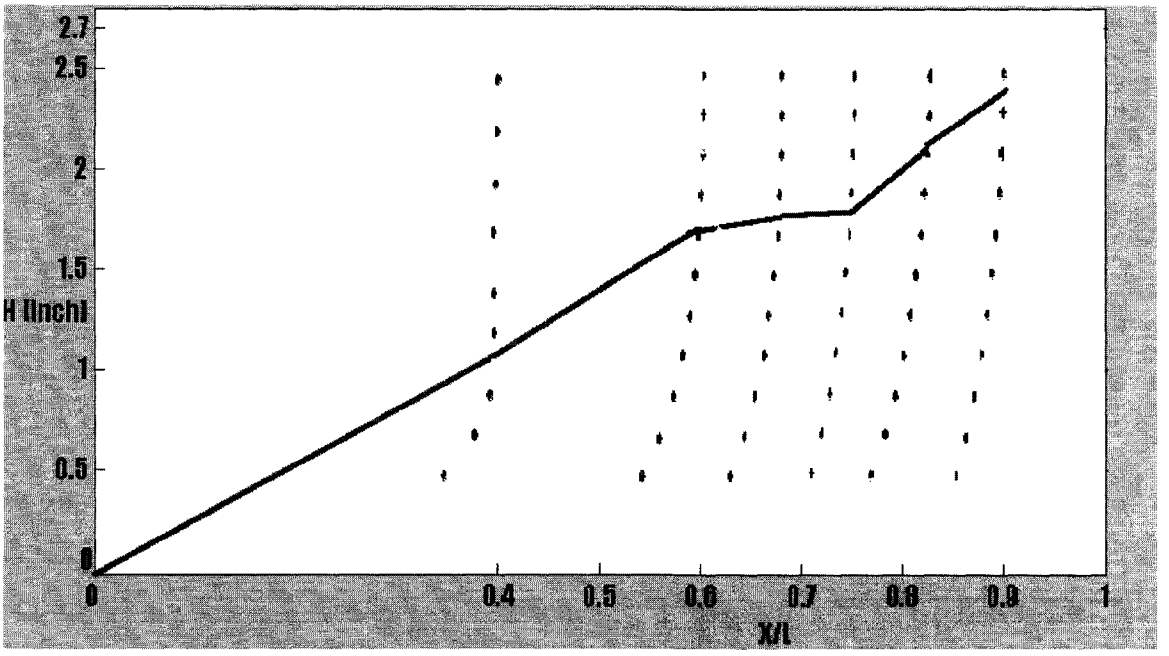

Figure 3. 3 Velocity profiles at 5 stations downstream of the elevated plate leading edge and measured boundary layer along the plate

3.2 Vehicle Models

3.2.1 Truck Model Design

There is no typical or classical truck model developed by previous works. In this study, the "rounded front" truck model is proposed following the idea of the Ahmed body used for passenger vehicles. It has the same size as the real shape truck model, which is 1:24 scaled down. The rounded front end is based on the scale of the Ahmed body in order to generate a strong three dimensional

displacement flow at the front. The slant angle at the back of the Ahmed body is kept as zero to maintain the box shape of the road truck at its back.

Typically, the ground clearance of a road-going truck is very large when compared to the thickness of a controlled boundary layer on the floor of a modern wind tunnel. Hence, the correct ground flow conditions have been considered less critical than for low-ground-clearance vehicle (sedan) [Barlow et al, 1999]. Usually a good boundary layer suction system can be used to improve the ground flow conditions. In this study, four simple stilts are utilized (the model body is above the boundary layer at the measuring position) to support the model body since the underbody flow condition is not the main concern.

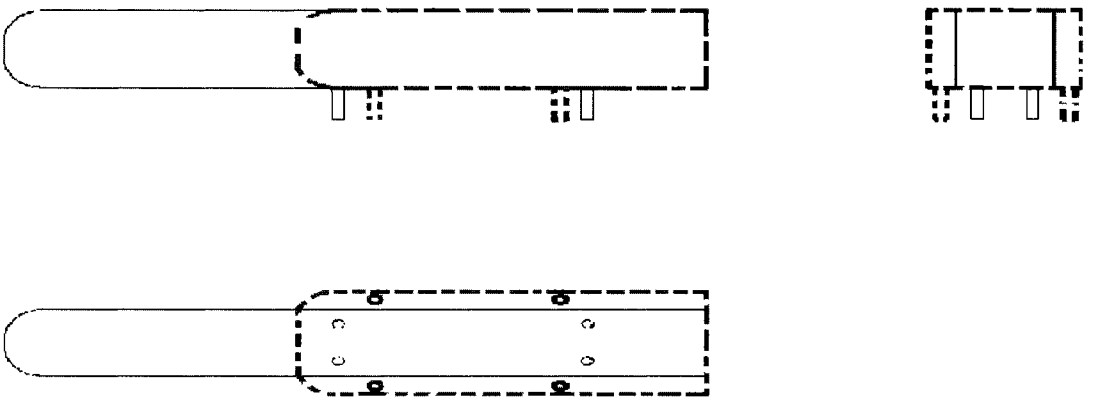

Figure 3.4 Rounded front model Current study (solid line) vs. Duell & George's work (dash line) [1999]

The proposed rounded front model is similar to the model used by Duell & George [1993, 1999]. As can be seen in Figure 3.4, other than the minor discrepancy of the

width, the main difference is that our model is about twice the length of Duell and Geroge's model.

3.2.2 Truck Models

In order to investigate the model shape effect, four truck models with various levels of model details are used in present study. Listed from simple to complex, they are:

- Rectangular block (1:24, wood)

  The rectangular block, similar to that used by Duell and George [1999], is used as an idealized bluff body. The details of this model are portrayed in Figure 3.5.

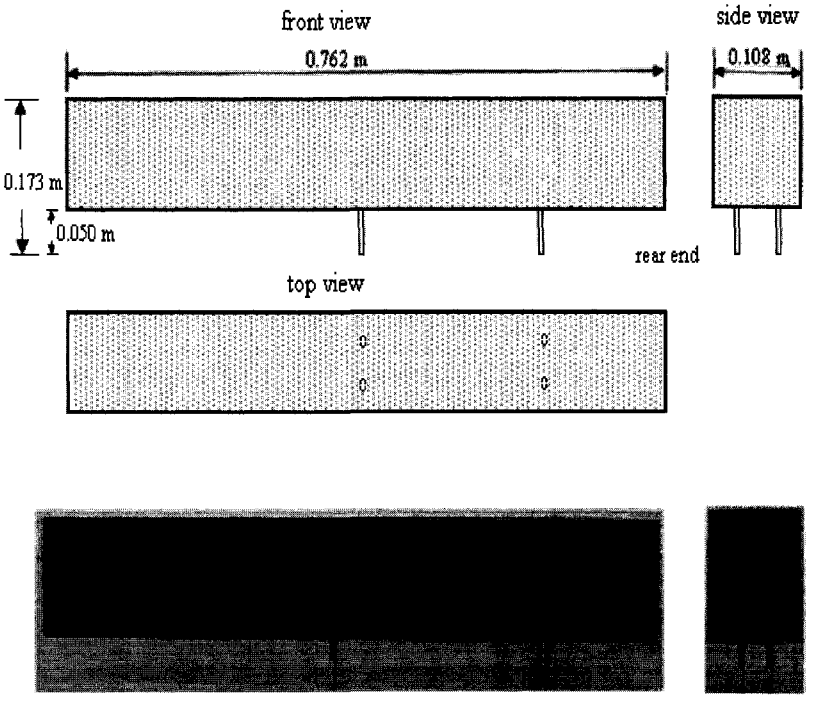

Figure 3.5 Three view drawings and the real picture of the rectangular block

- Rounded front model (1:24, wood)

This proposed model is a modification of the rectangular block. The only difference is the rounded front end, see Figure 3.6. The ratio of the radius to body height is based on that used in the Ahmed body [Ahmed et al, 1984].

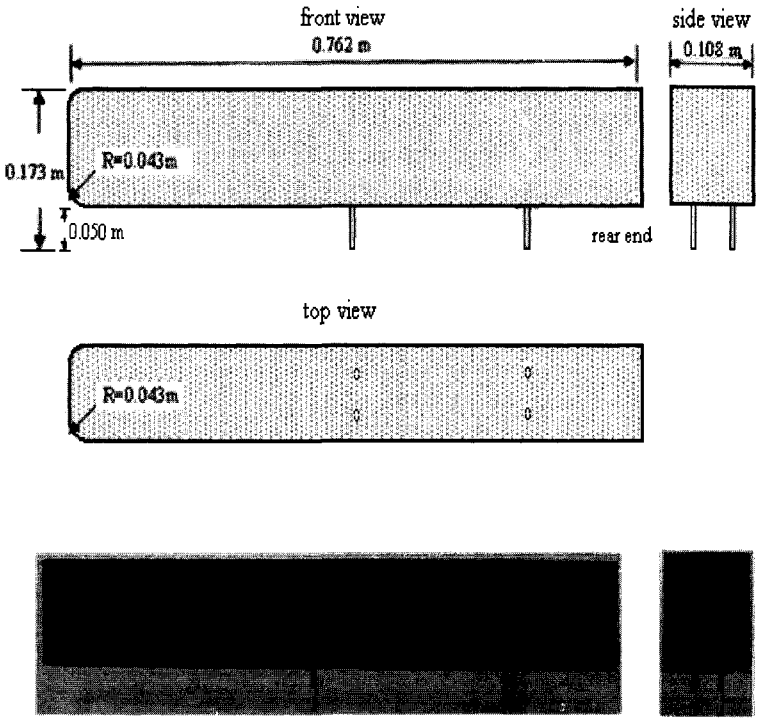

Figure 3.6 Three view drawings and the real picture of the rounded front model

- Generic model (1:24, foam)

This plastic paper covered model is constructed based on the gross dimensions of the real shape model. It is of uniform width, and the "wheels" are replaced by slim rectangular blocks. The overall weight of this model (0.7kg) is much less than the previous two wooden ones (1.9kg). See Figure 3.7 for details.

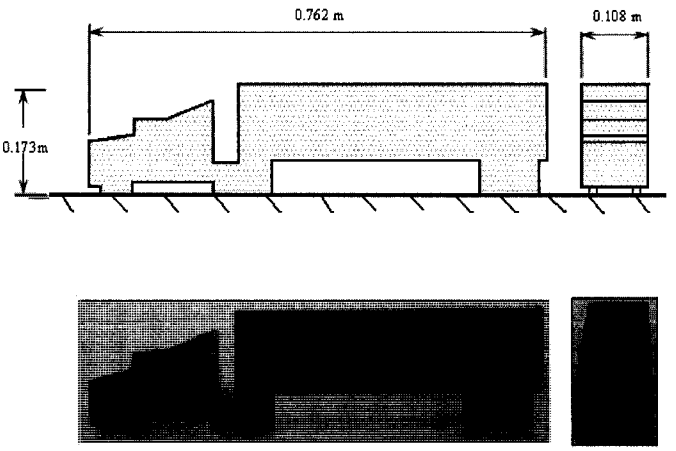

Figure 3.7 Side and front views and the real picture of the generic model

- Scaled specific model-Kenworth T-600B

  (1:24 die—cast metal & ABS resin)

  The detailed model truck is a 1:24 scale replica produced from original engineering drawing of Kenworth and Great Dane, which represents a typical tractor-trailer type on the North American road. Figure 3.8 shows the side and front views of this model.

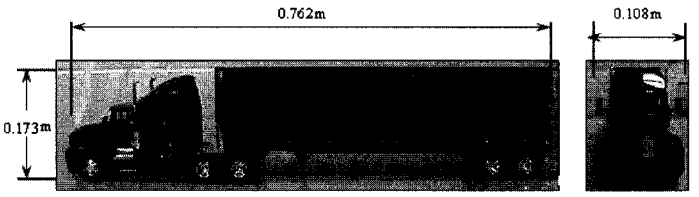

Figure 3.8 Side and front views of scaled specific model

The model has a frontal area of 0.0187m^2 and the cross sectional area of the wind tunnel is 0.5806 m^2, thus the blockage ratio is 3.2%. With the elevated plate, this value goes up to 4.1%, which is still less than the upper limit of 5% blockage ratio, beyond which corrections of blockage effect should be applied [Hucho 1998].

Table 3.2 shows the comparison of surface roughness of the three simplified truck models. The data was collected using a SJ-2019 Surface Roughness Tester. As can be seen from the table, the overall relative surface roughnesses of the three simplified truck models are all in the order of 10^{-6}.

Table 3.0.2 Relative surface roughness of the simplified truck models (rectangular block, rounded front model and generic model)

Relative roughness: *e/D* *	Top	Front	Side	Overall
Rectangular block	6×10^{-6}	5×10^{-6}	7×10^{-6}	6×10^{-6}
Rounded front model	10×10^{-6}	7×10^{-6}	8×10^{-6}	8×10^{-6}
Generic model	13×10^{-6}	10×10^{-6}	5×10^{-6}	9×10^{-6}

Note: *e* is the absolute magnitude of the surface roughness, which was collected using the SJ-201P surface roughness tester (Unit: μm); the magnitude of the model height D=177.8mm.

3.2.3 Sedan Model

The sedan model is made of die cast metal with plastic parts. The prototype, Nissan skyline R34 GT-R, is also commonly seen on the road in North America. See Figure 3.9 for model details.

Scaled specific model-Nissan skyline R34 GT-R (1:24 scale)

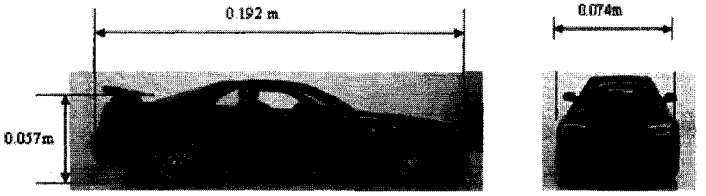

Figure 3.9 Side and front view of sedan model

3.3 Hot-Wire System

Hot-wire anemometry (HWA) is likely to remain the principle research tool for most turbulent air flow studies. It is based on convective heat transfer from a heated wire or film element placed in a fluid flow. Any change in the fluid flow condition that affects the heat transfer from the heated element will be detected virtually instantaneously by a constant-temperature HWA system. HWA is used in this study to quantify the flow fluid around the truck model. Figure 3.10 is a photo of the hot-wire system used in this study.

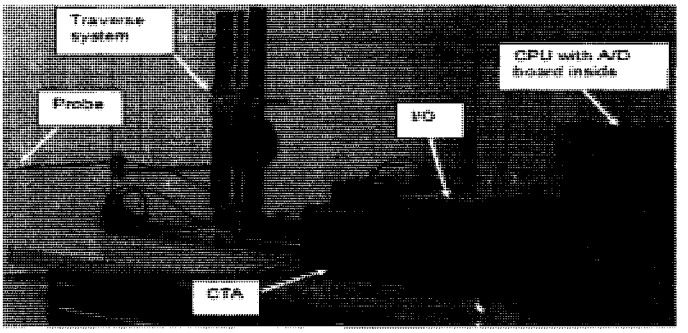

Figure 3.10 Hot-wire system [CTA: Dantec Streamline 55C90, I/O: shielded I/O connector block for DAQ devices, A/D: PCI-6071E]

Constant Temperature Anemometer (CTA)

The current hot-wire anemometer is the Dantec Streamline® 55C90 CTA modules installed within a Dantec 90N10 frame. The 55C90 module contains a constant temperature anemometer and a signal conditioner. The 90N10 frame is used as power supply, controller and a temperature transducer.

PCI-6071E A/D board

The current A/D converter installed on the motherboard of the CPU is National Instrument PCI-6071E. It is a multifunction data acquisition board which has a 12 bit resolution.

SCB-68

The communication between the hot-wire anemometer and the A/D board is made possible via a National Instrument SCB-68 shielded I/O connector block. It is for data acquisition devices with 68-pin connectors which can provide rugged, very low-noise signal termination.

Traverse system

The traverse system for the hot-wire probe and the temperature probe support and movement is an Animatics® SmartMotor SM2315D. It is mounted downstream of the tested truck model and fixed on the wind tunnel floor using screws. It can be controlled manually or by computer using the 2D smartmotor motion program.

Calibration

The calibration of hot-wire probe is performed by using an air jet located in Room

B15 Essex Hall coupled with a Pitot static tube as well as a digital manometer for velocity measurement reference. Before each experiment, the calibration is conducted to establish the relationship (4^{th} order polynomial) between the air velocity and the output voltage of the hot-wire probe. The pitot tube system is replaced by a new auto calibrator from Dantec during the remaining work.

Data acquisition

Data acquisition software developed by Rui Liu will be utilized with modifications according to different experimental tasks. The motions of the traverse system and data collection are programmed to be automatically carried out. The motion control of the single normal probe and data acquisition is well coordinated; the task is accomplished with two programs (see Appendices C, D).

3.4 Flow Visualization Setup

To assist in identifying the truck wake structure, flow visualization was performed by using fog machine and tuft grids. As can be seen in Figure 3.11, the fog machine is placed beneath the wind tunnel board, and fast dissipate solution is used. The smoke was injected in front of the model.

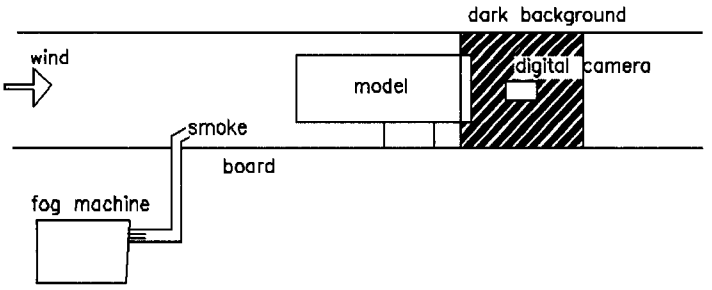

Figure 3.11 Experimental arrangement for smoke visualization

Visualization of tuft grid is depicted in Figure 3.12. The tuft grid is mesh of wire, with tiny string tied at each intersection. Two sets are used, one with 1 inch grid size, the other one with 1/3 inch grid size.

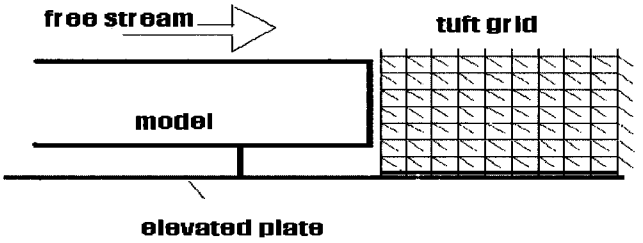

Figure 3.12 Experimental arrangement for tuft visualization

(vertical central plane)

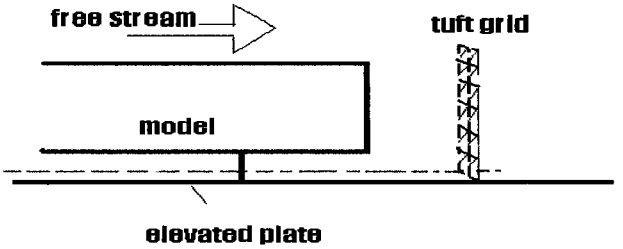

Figure 3.13 Experimental arrangement for tuft visualization

(vertical transverse plane)

Chapter 4 Results and Discussion

4.1 Shape Details Impact

The first series of wind tunnel tests aims at studying the impact of model details on the wake characteristics of a truck model. The truck model was placed right at the central line of the wind tunnel ground board, see Figure 4.1. The testing area covers the vertical central plane right behind the truck model.

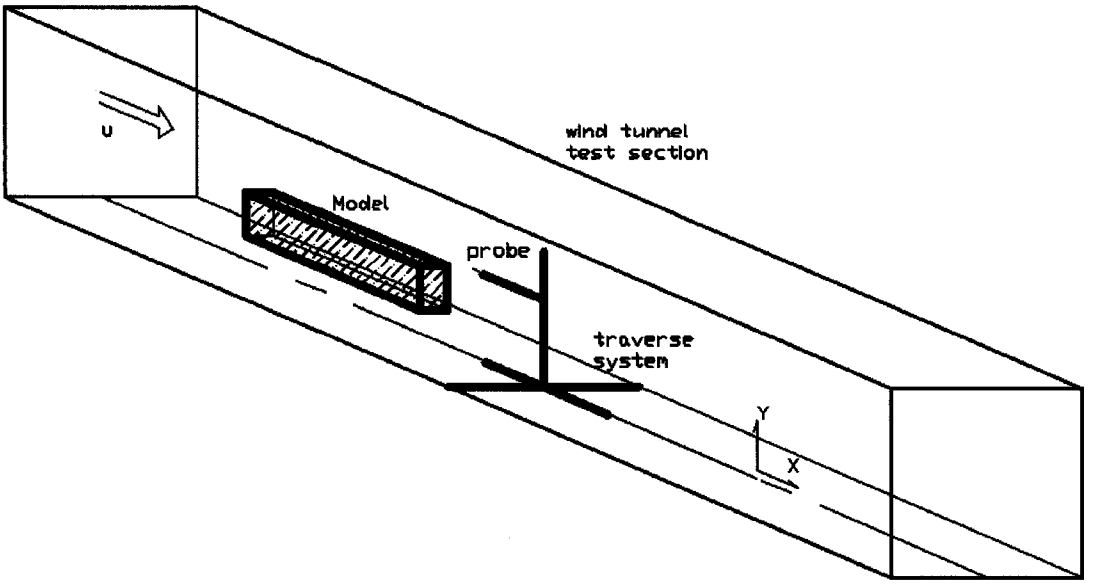

Figure 4. 1 Experimental arrangement for studying wake of the truck model: single truck-vertical central plane without elevated plate

During the tests, the single hot-wire probe was mounted (along with a temperature probe for correcting the fluid density and viscosity change from the calibrated conditions) on the traverse system downstream of the model, the movement of which was controlled by a smartmotor program.

The grid used for hot-wire measurement is illustrated in Figure 4.2. The area covered is 5.25 inch (0.133m) in width and 5 inch (0.127m) in height. The starting position of the probes is 1 inch (0.025m) downstream from the model base in order to avoid potential probe breakage. The height of the area covered by the testing grid is the same as that of the model body.

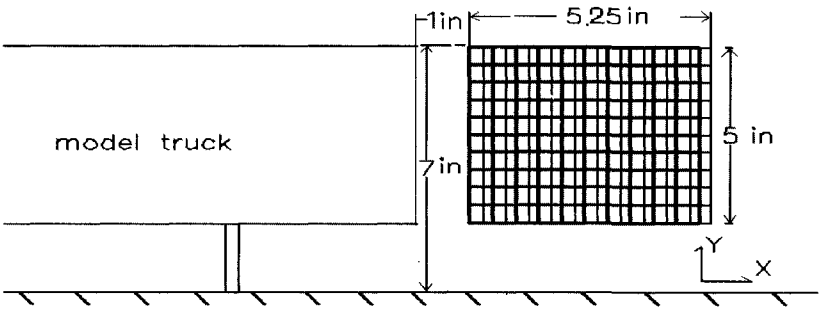

Figure 4.2 Grid for data collection

For each model, two grid systems were used. Each grid is 11 by 11, resulting in 242 measurement points in total. The two grid systems span the same vertical range, and overlap 0.25 inch (0.635m) in the horizontal direction. The reason for using this two-grid-system scheme is to make sure the suggested trend of near wake mean velocity distribution (see Figure 4.7) exists in single grid as well as in the two-grid-system. During the experiment, at each grid point, the instantaneous velocity was recorded over a period of approximately 28 seconds. The data was sampled at 75 kHz and subsequently, low-pass filtered at 30 kHz. The sampling number was chosen to be 2,097,152 to ensure that no important information was missed in the early stage measurement. The sensitivity results showed that this

value is sufficient, the ideal sampling number is around 1,600,000 (See Appendix C and Table 4.1 for details).

Table 4.0.1 Parameters in the first series of tests

Sampling number	Sampling frequency	Free stream wind speed	Max Reynolds number	Blockage ratio
2097152	75kHz	14m/s	7x10E5	3.2 %

As depicted in Figure 4.2, there are 11 lines in the horizontal direction of the grid system. The distribution of the mean velocity at each line can be determined from measured data along these lines. The near wake mean velocity distribution along some of these 11 lines is similar to that obtained by Duell and George [1993], as can be seen in Figure 4.4. Therefore, the recirculation length X_r was deduced from the distance between the model rear end and the grid point where the first derivative of the velocity with respect to streamwise distance x is zero and the second derivative is positive. In other words, X_r is the distance from the model rear end to the point where the slope of velocity profile in the streamwise direction is 0 and curvature is upward (positive), see Figure 4.4. This stagnation point [Duell & George, 1993] can be obtained via curve fitting.

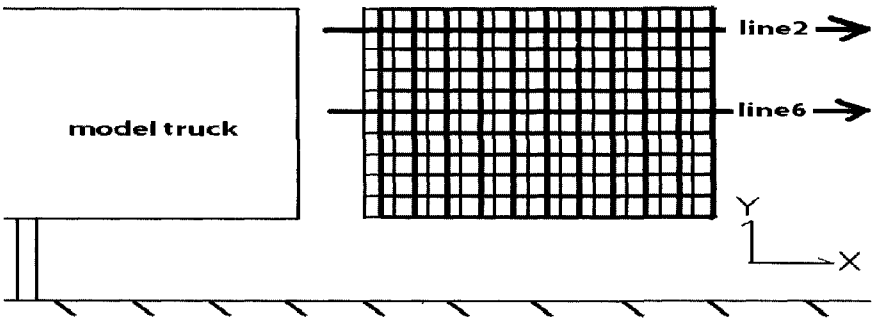

Figure 4. 3 Wake centerlines

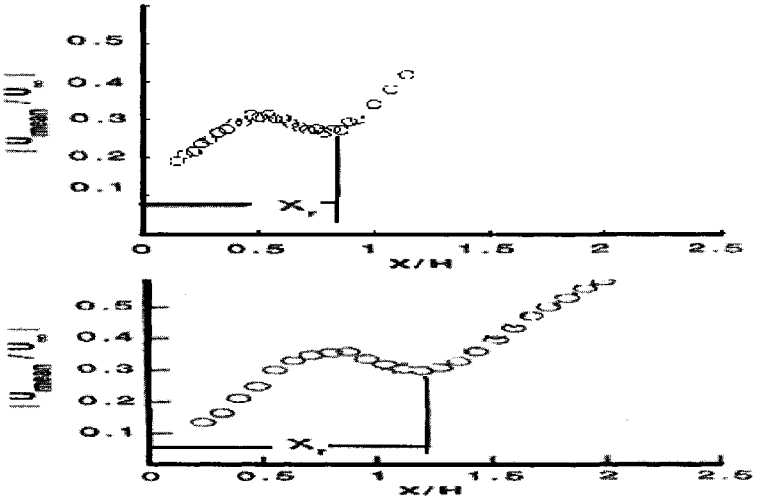

Figure 4. 4 Near wake time averaged velocity distribution at the vertical central plane and recirculation length

Current study (upper one) vs. Duell & George's work [1993]

In Figure 4.5, the bubble shape in the wake of the rectangular block at $Re=7\times10^5$ (based on the model length) is illustrated. Figure 4.5(a) consists of a collection of stagnation points along the horizontal lines in the measuring grid. In this case, only four measuring lines have the trend shown in Figure 4.4. The largest X_r is chosen as the recirculation length, which is found to be 0.64 times of the model height by

curve fitting. The mean velocity contour and derived bubble shape for the four truck models at Re=7×10^5 are plotted in Figures 4.5 – 4.8. Table 2 presents the summary of recirculation length X_r of these different truck models obtained from the current work.

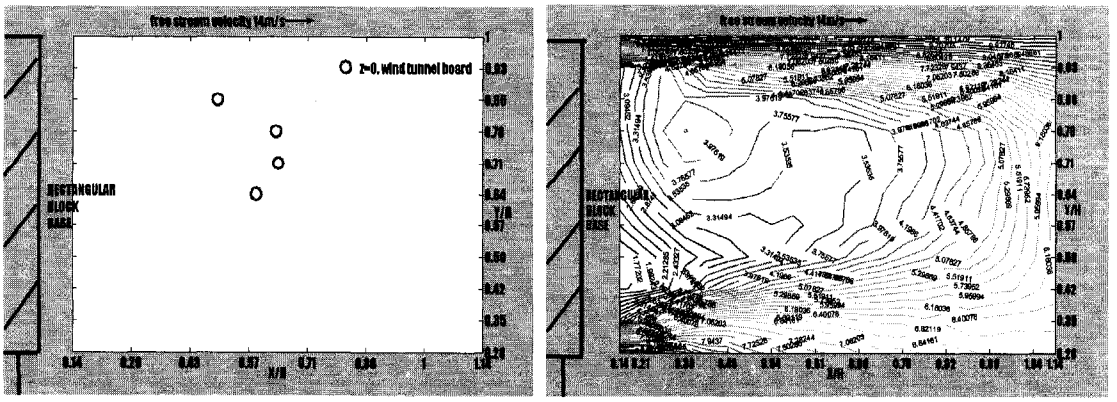

(a) (b)

Figure 4.5 Bubble shape of the rectangular block and corresponding mean velocity contour in the wake at Re=7×10^5

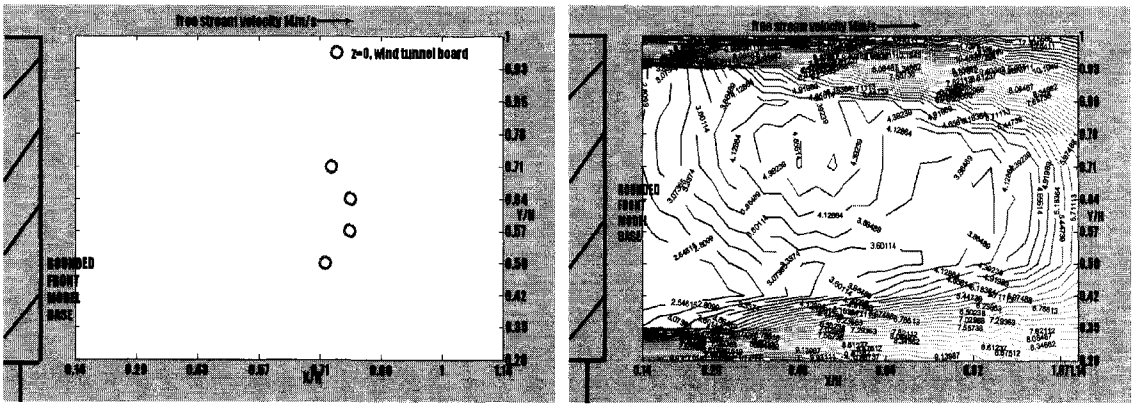

(a) (b)

Figure 4.6 Bubble shape of the rounded front model and corresponding mean velocity contour in the wake at Re=7×10^5

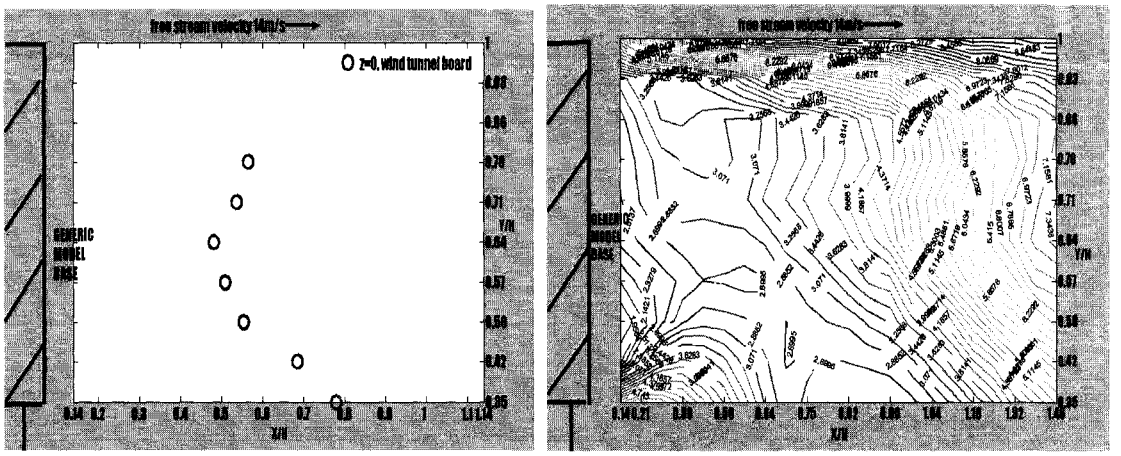

(a) (b)

Figure 4. 7 Bubble shape of the generic model and corresponding mean velocity contour in the wake at Re=7×10^5

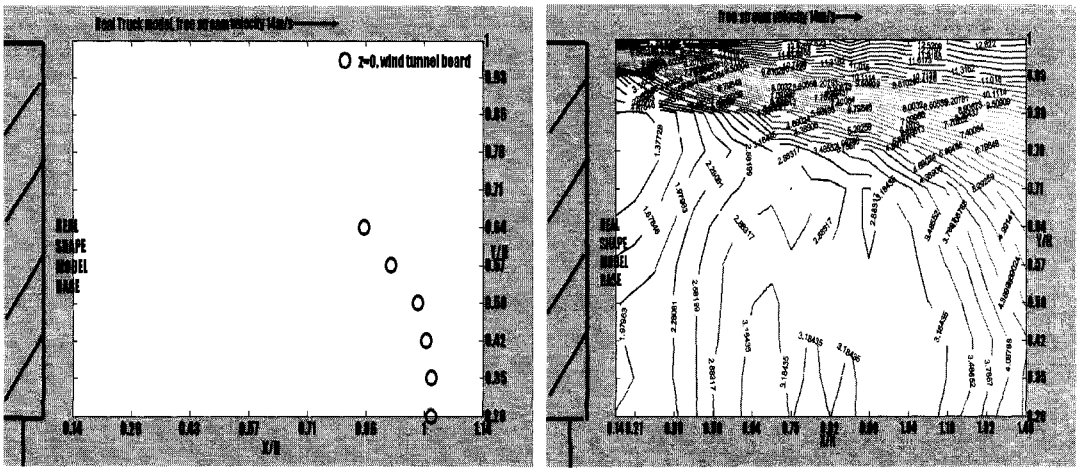

(a) (b)

Figure 4. 8 Bubble shape of the real truck model and corresponding mean velocity contour in the wake at Re=7×10^5

Table 4.0.2 Recirculation length of the models at $Re=7\times10^5$

Model/ Recirculation length	RB	RF	GM	RS
X_r/H	0.64	0.78	0.78	1.02

Note: RB=Rectangular Block, RF=Rounded Front model, GM=Generic Model, RS=Real Shape model.

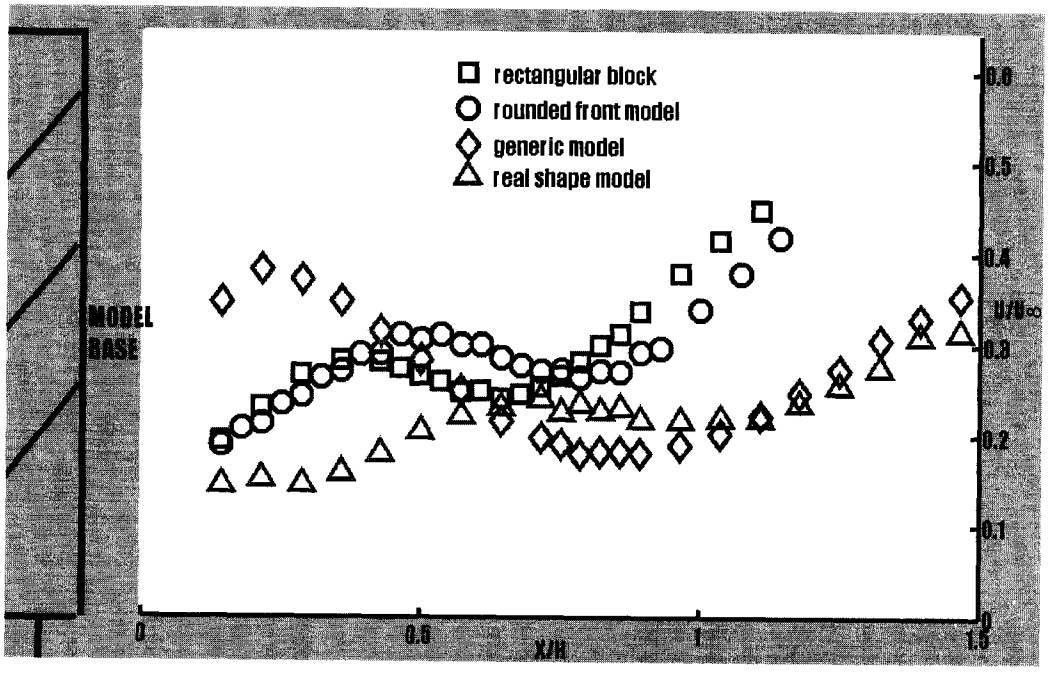

Figure 4.9 Streamwise velocity distribution at the horizontal line where recirculation length can be determined

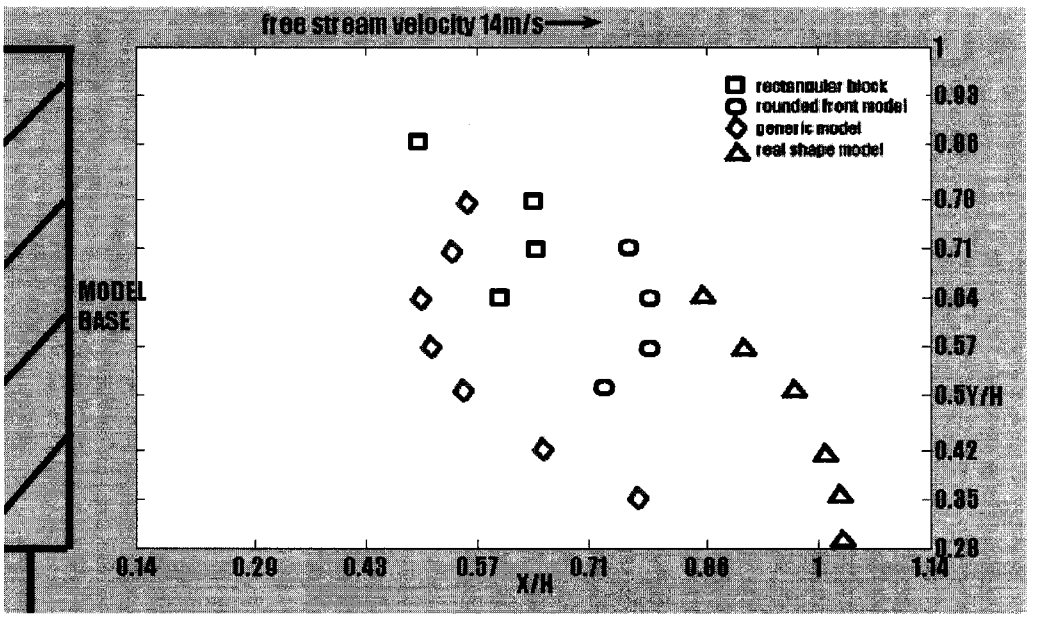

Figure 4. 10 Comparison of bubble shapes of all the truck models

The shapes of the wake bubbles as shown in Figures 4.5 and 4.6 are similar to that obtained by Duell and George [1999] (compare Figures 4.5 and 4.6 with Figure 2.12). For the rounded front model and the rectangular block, the extents of the wake bubble are in the proximity of the horizontal centerline of the models. The difference between these two sets of results is that the rounded front model has a relatively larger (longer) near wake region than that of the rectangular block, i.e., a recirculation length of 0.78 versus 0.64 —the reason may be that the flow separation is delayed for the rounded front model.

In Figure 4.8, the bubble tip of the real truck model moves downward to the ground. The same trend may be inferred from the corresponding flow visualization shown in Figure 4.11.

The largest discrepancy exists in the generic model case— two bubbles can be identified in the near wake with the upper one being relatively small. The demarcation of these two bubbles is near the horizontal centerline. As for the shape, the lower bubble appears to have a different curvature, i.e., concaving downstream.

To sum up, the real shape model has the longest near wake region in the streamwise direction, while the rectangular block has the shortest. The length of the wake bubble of the rounded front model is literally identical to that of the generic model, and they are larger than the wake bubble of the rectangular block but shorter than that of the real shape model. Concerning the shape of the wake bubble, the bubble moves downward and away from the model base as more model details are included. The generic model appears to show a double- (or dual-) bubble, but this has not been confirmed in the real truck model case. See Figure 4.7 and 4.8 for details.

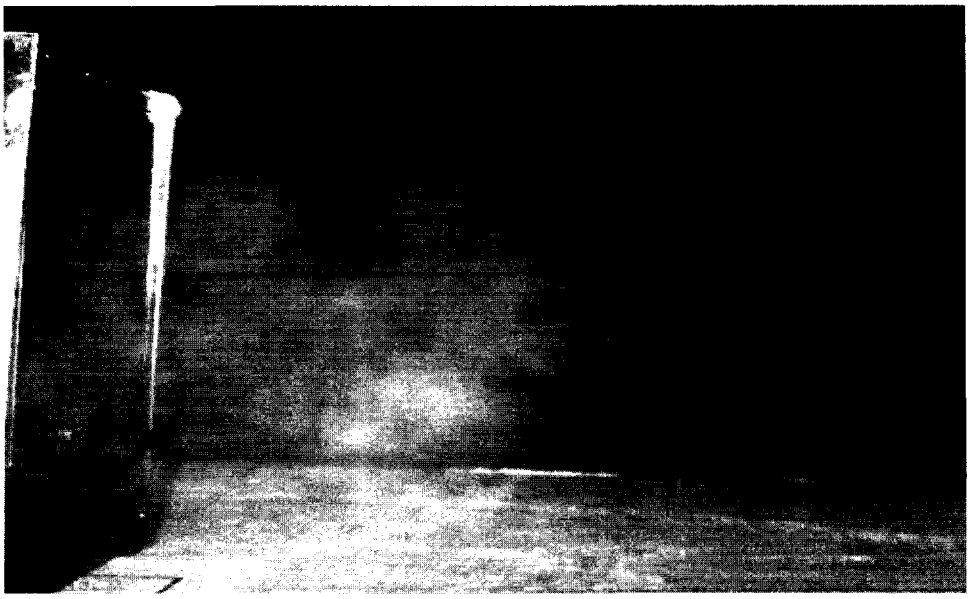

Figure 4.11 Smoke visualization of wake flow behind a real shape truck model

4.2 Elevated Plate Impact

The remainder of the wind tunnel tests is with an elevated plate. Table 4.3 shows the parameters used. There are minor changes compared with Table 4.1.

Table 4.0.3 Parameters in the rest series of tests

Sampling number	Sampling frequency	Free stream wind speed	Max Reynolds number	Blockage ratio
1600000	75kHz	14m/s	7x10E5	4.1%

First of all, the same measurements as in the first series have been done on the elevated plate in order to find out the impact of ground simulation on the results (Figure 4.12).

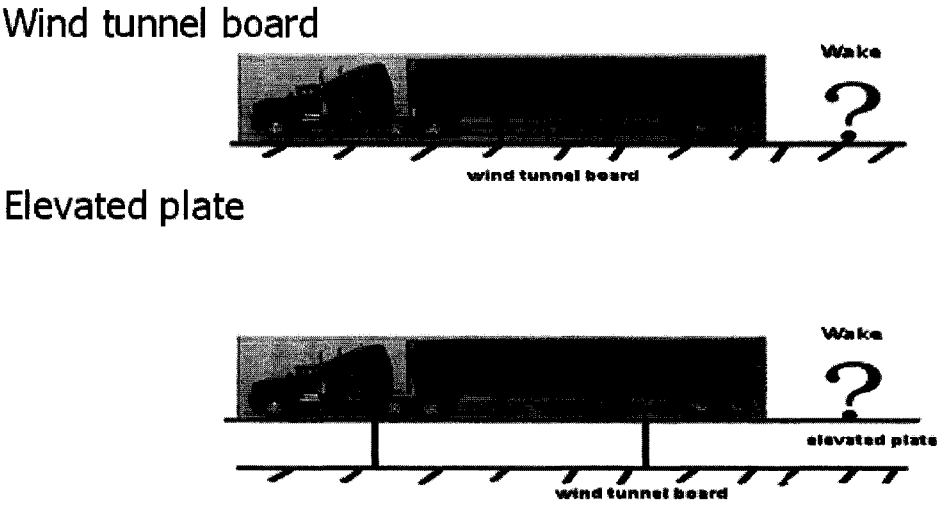

Figure 4. 12 Different ground simulations

The results obtained in the first series of tests are in the central plane which is plane z=0.

As mentioned before, the hotwire measurement in the first series of tests has been repeated after the elevated plate is applied. Figure 4.13 shows the bubble shape of all the four models under two different ground simulations.

Generally speaking, there is not much difference between two sets of results regarding the central plane bubble shape despite minor discrepancies, which somehow proves the effect of boundary layer is small, see Appendix A for details.

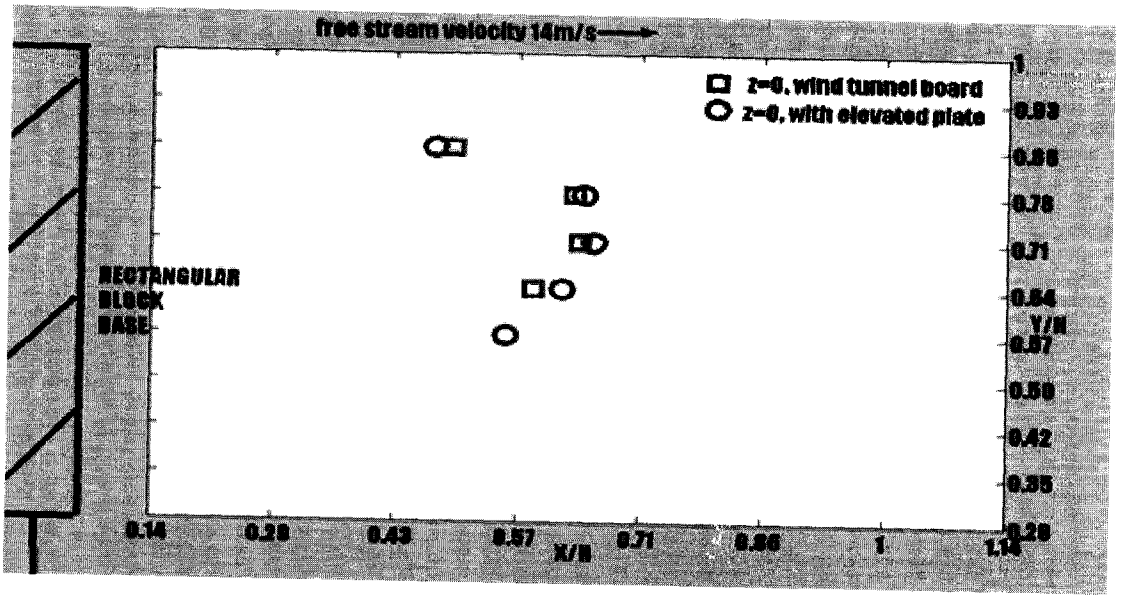

Figure 4. 13(a) Bubble shape of the rectangular block

wind tunnel board vs. elevated plate

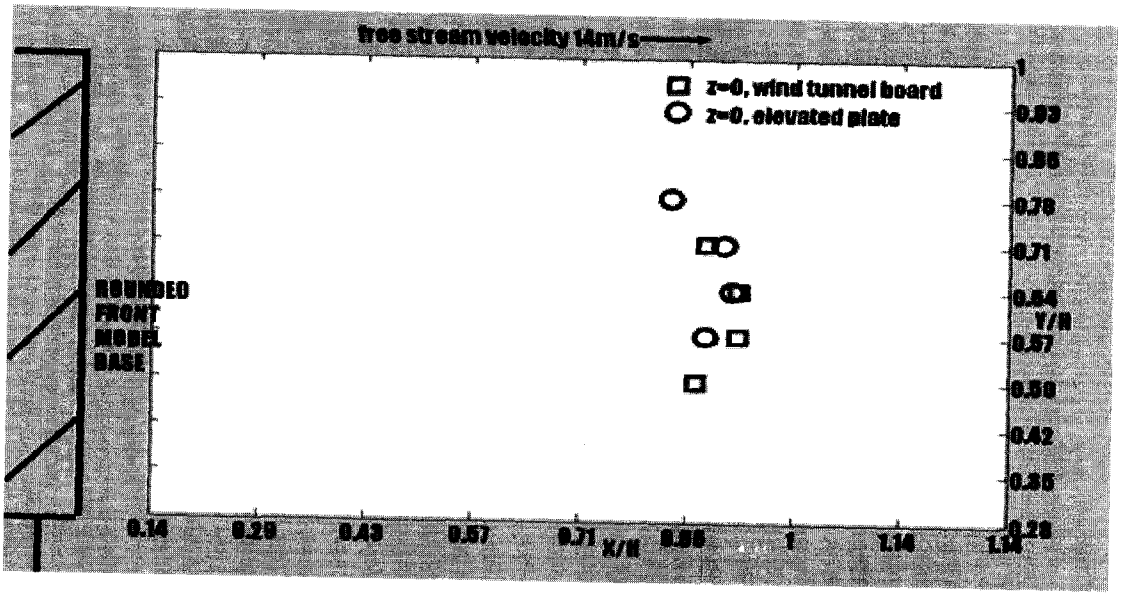

Figure 4.13 (b) Bubble shape of the rounded front model

Wind tunnel board vs. elevated plate

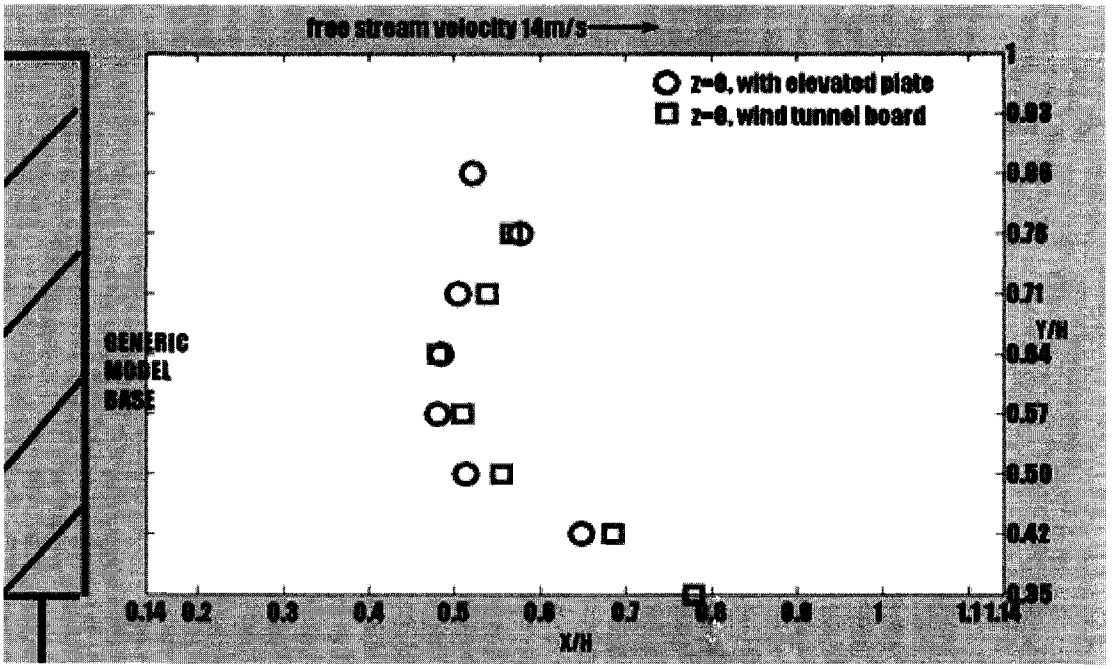

Figure 4.13 (c) Bubble shape of the generic model

Wind tunnel board vs. elevated plate

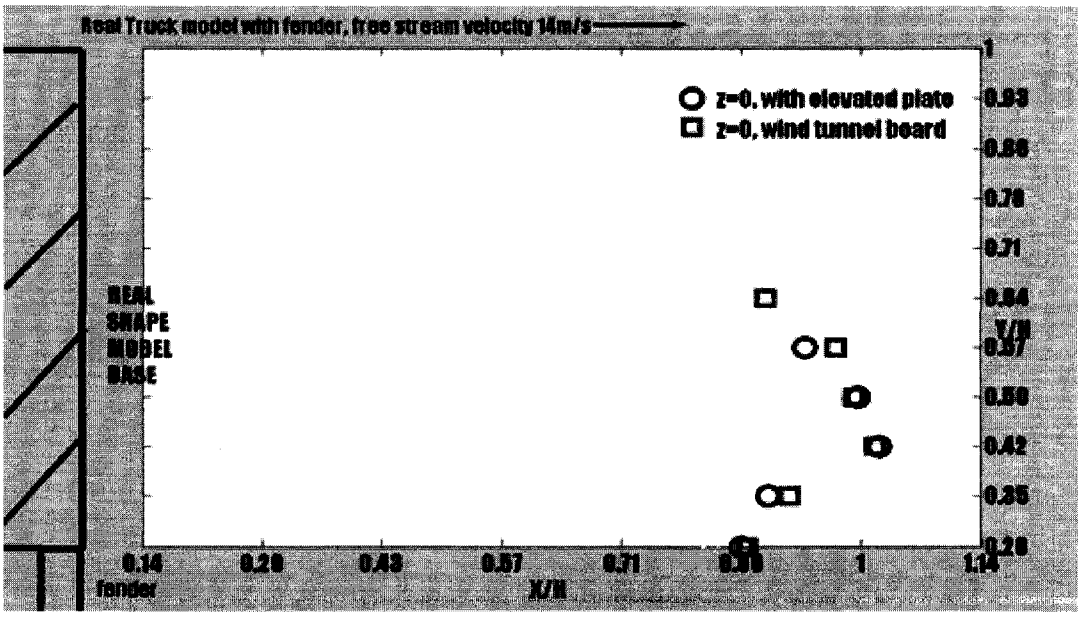

Figure 4.13 (d) Bubble shape of the real shape model

Wind tunnel board vs. elevated plate

For the remaining series of tests, the real shape model has been changed to a similar model with fender. It seems that for the recirculation length, there is no difference.

See Table 4.4 for comparison of the two ground simulations (with and without elevated plate) regarding recirculation length.

Table 4.0.4 Recirculation length of the models ($Re=7\times10^5$, with/ without elevated plate)

Model/ Recirculation length	RB	RF	GM	RS (new model with fender)
X_r/H	0.64/0.66	0.78/0.78	0.78/0.65	1.02/1.02

4.3 Three Dimensional Wake Bubble

Afterwards, the focus has been placed on the 3D characteristics of the wake bubble, in other words, besides measuring in the central vertical plane, the side vertical planes behind the truck are also our interest, see Figure 4.14.

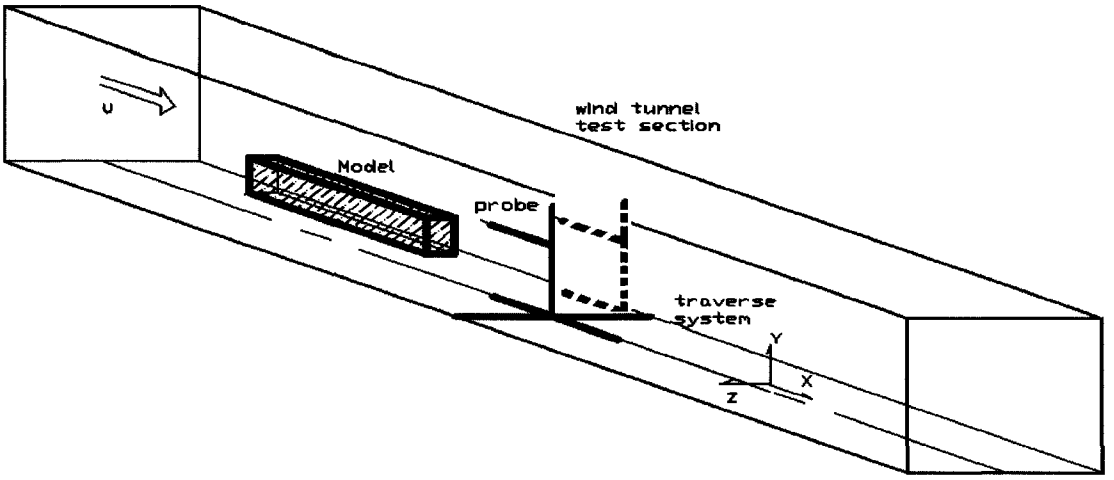

Figure 4. 14 Experimental arrangement for studying wake of the truck model: single truck case-vertical side planes

The three dimensional characteristic of the wake bubble is also a main concern in this study. The wake region of the truck models has been divided by several vertical planes. Due to the symmetry of the incoming flow throughout the truck model, only the positive side (z=w/8, w/4, 3w/8, w/2) have been investigated, see Figure 4.15.

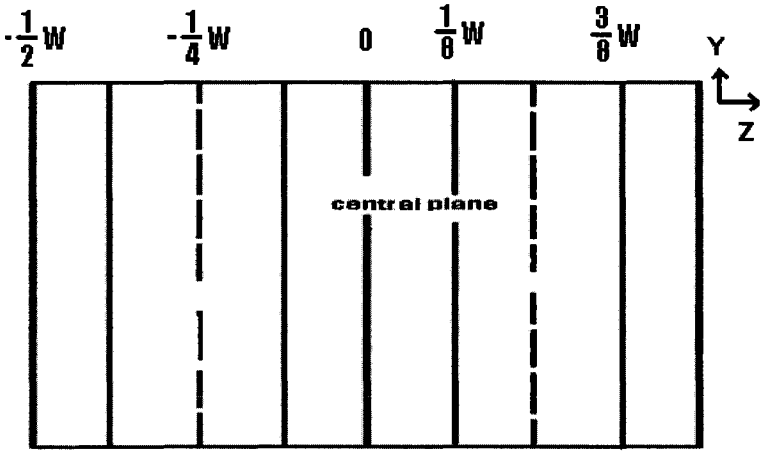

Figure 4. 15 Back view of vehicle model

It turned out that at some of the vertical planes, there are also bubble shapes that can be deducted. Basically, the bubble shrinks and vanishes as the plane moves from the central plane (z=0) to the side edge (z=w/2), the bubble is fully three dimensional. See Figure 4.16 for more information.

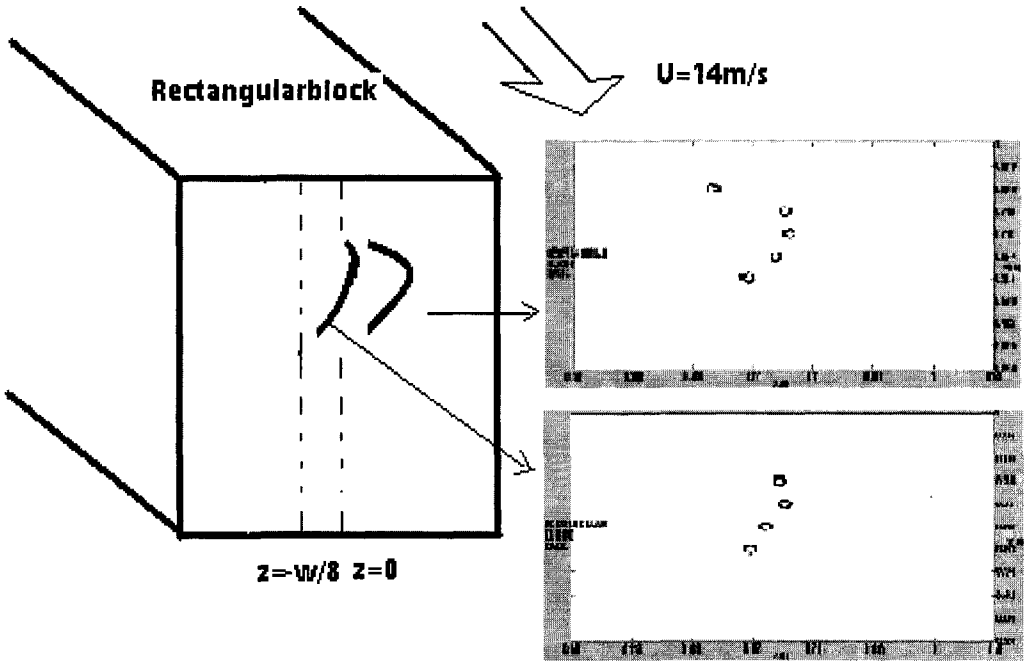

Figure 4. 16 (a) Three dimensional bubble of rectangular block

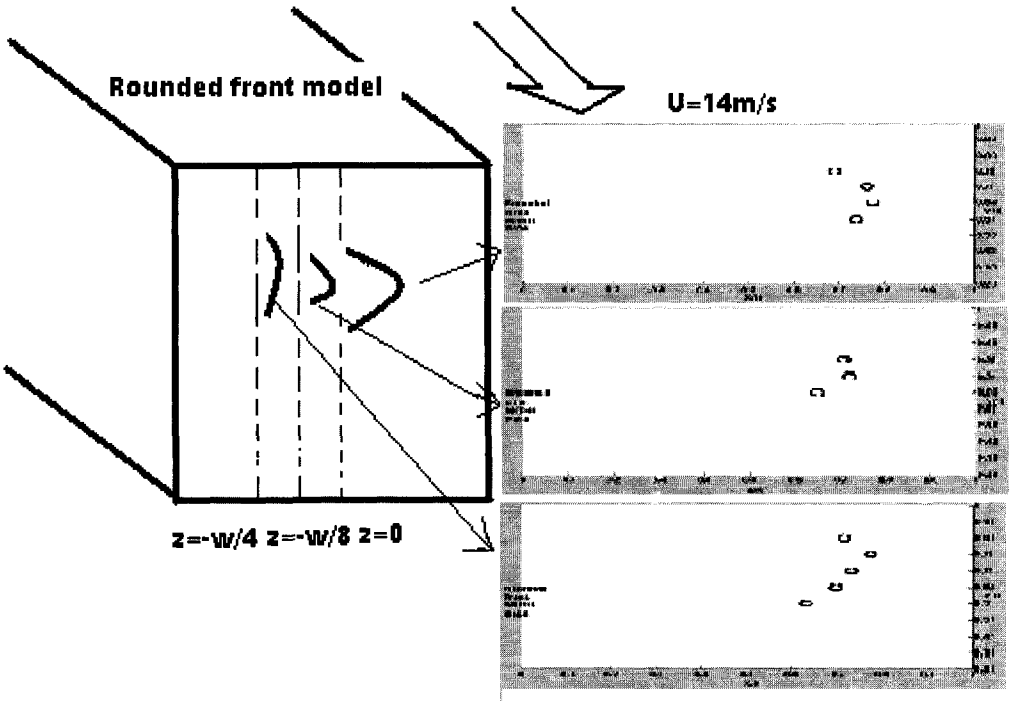

Figure 4.16 (b) Three dimensional bubble of rounded front model

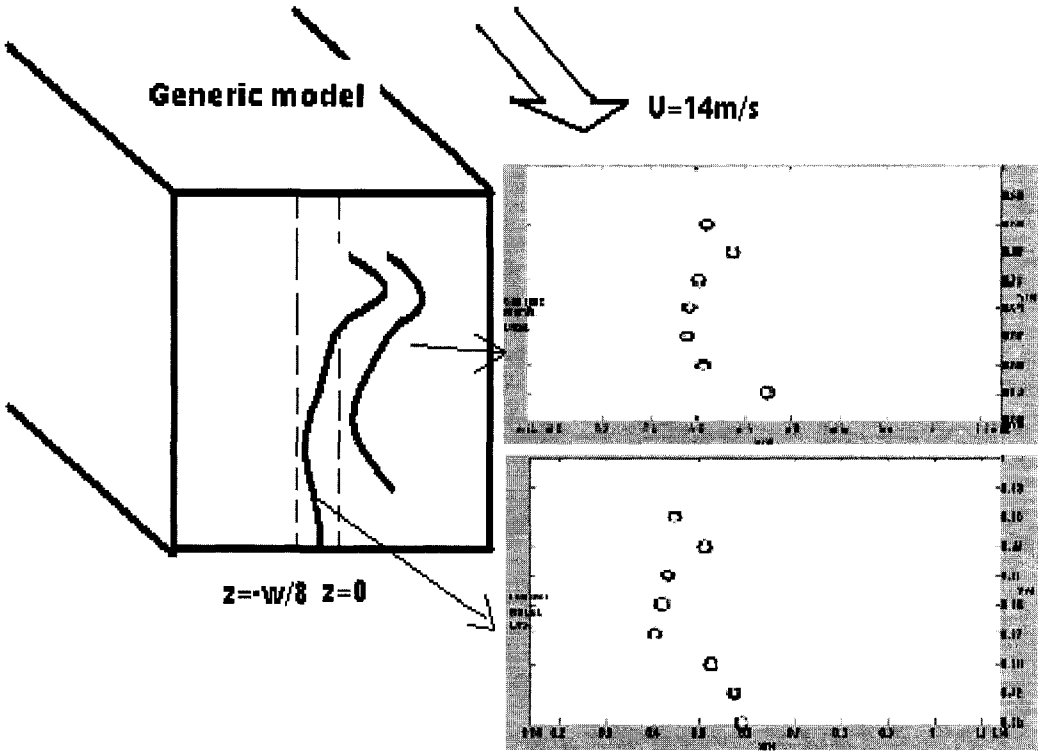

Figure 4.16 (c) Three dimensional bubble of the generic model

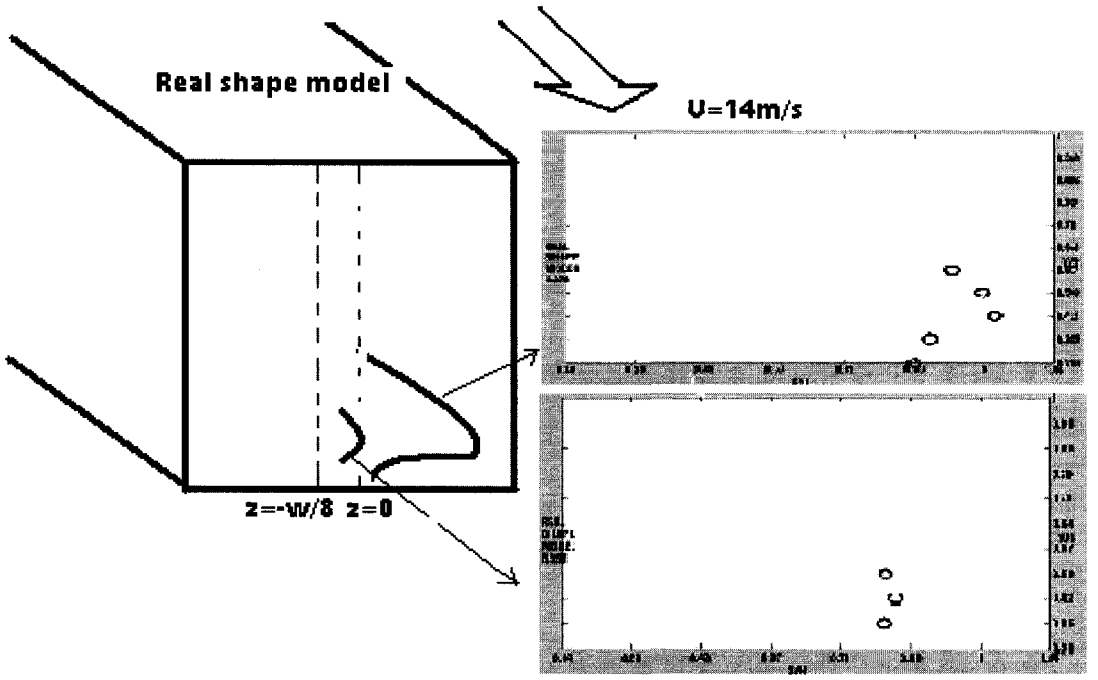

Figure 4.16 (d) Three dimensional bubble of real shape model

Table 4.0.5Detection of bubble for different truck models

location	Rectangular block	Rounded front model	Generic model	Real truck model
Central plane Z=0	Yes	Yes	Yes	Yes
Z=±1/8W	Yes	Yes	Yes	Yes
Z=±1/4W	No	Yes	No	No
Z=±3/8W (close to the side edge)	No	No	No	No

It seems that the rounded front model has the largest bubble region, which extends to z=±w/4. While for the rest of the models, it extends to z=±w/8, which means the bubble vanish somewhere between w/8 and w/4.

4.4 Sedan and Truck in Tandem Arrangement

A sedan model is introduced, and sedan and truck in tandem case has been studied. The result shows the bubble shrinks at the central plane (z=0) while extends at the side plane (z=±w/8) as the spacing between the leading sedan and followed truck decreases. Furthermore, the scope of the bubble does not change because of the presence of the leading sedan. See Figure 4.18 for more details.

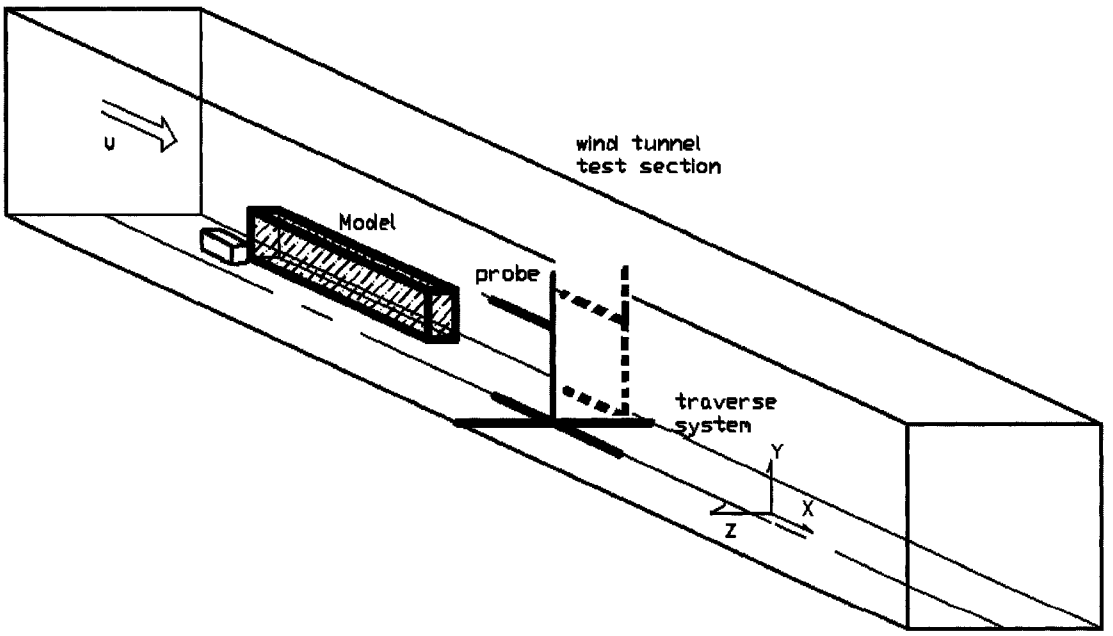

Figure 4. 17 Experimental arrangement for studying wake of the truck model: sedan and truck in tandem case

Table 4.6 presents the existence of bubble for the sedan and truck in tandem case.

Table 4.0.6 Detection of bubble on the real shape model

location	Spacing: 0.5H	Spacing: H	no sedan
Central plane Z=0	Yes	Yes	Yes
Z=±w/8	Yes	Yes	Yes
Z=±w/4	No	No	No

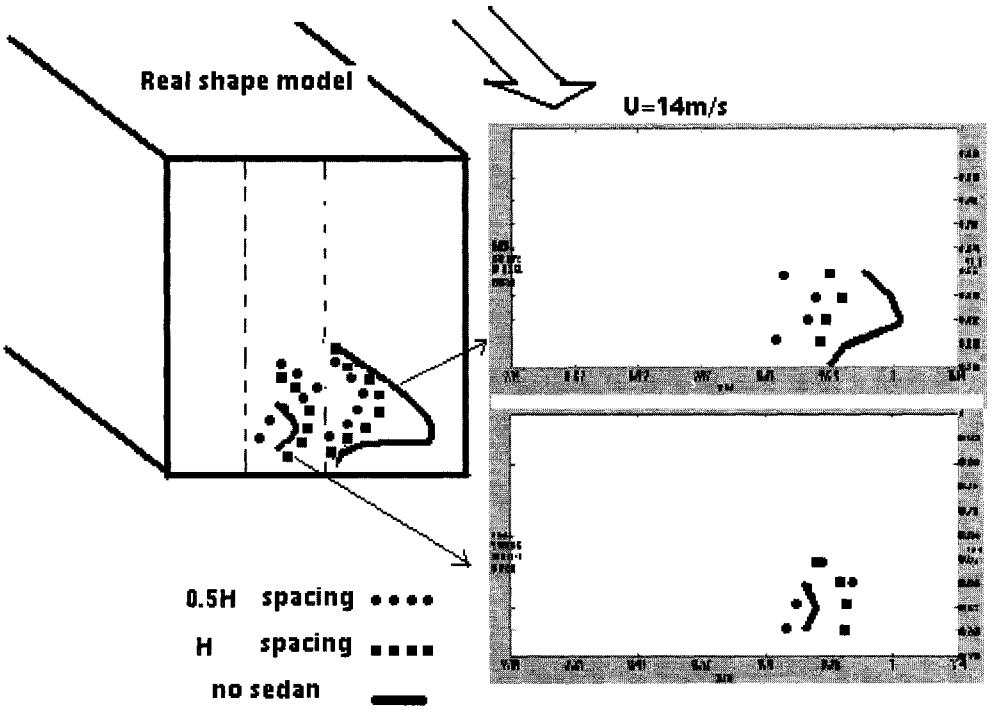

Figure 4. 18 Three dimensional bubble of real shape model:

Sedan and truck in tandem

4.5 Reynolds Number Effect

The Reynolds number effect has also been investigated.

The last set of experiments concerns the Reynolds number effect. All the results presented so far in this study are under the condition of 14 m/s free stream velocity, which corresponds to approximate 3km/h for the real life scenario. Thus, extrapolating the result is necessary. Based on the turbulence manipulation method (Wiedeman, 1989), we conducted a set of measurements attempting to find a way to reduce the Reynolds number effect in this study.

A perforated plate is applied, the detailed dimension is shown in Figure 4.19, and it basically covers the whole cross section of the wind tunnel.

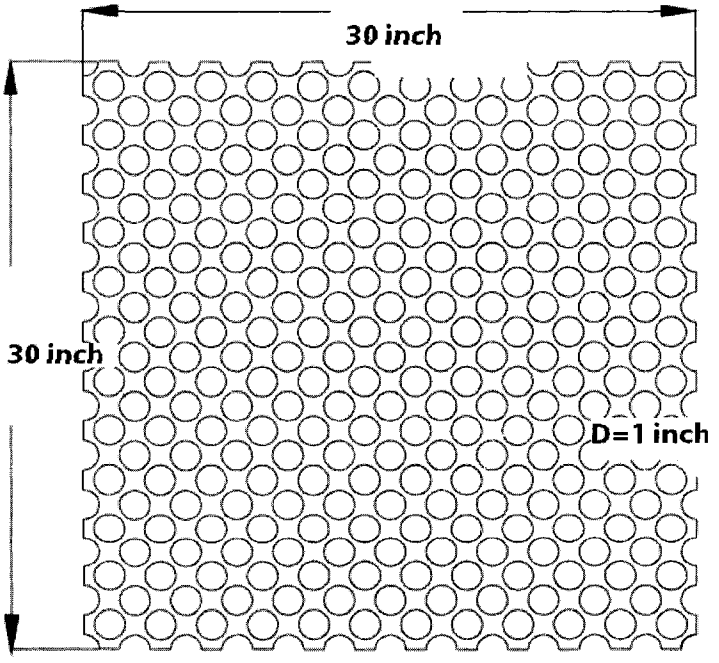

Figure 4. 19 Application of perforated plate

Here we define the tests with no screen mounted at the wind tunnel inlet as "smooth flow" case, if screen is on, then it is "turbulent flow" case. The distance between the screen and the front of the truck model is about 30 inch; the turbulent intensity generated is 3.0% as measured. Table 4.7 shows the cases tested for extrapolation, for both "smooth flow" and "turbulent flow" cases, the recirculation lengths are almost identical within the range of Re=4×10^5 to 7×10^5.

Table 4.0.7 Extrapolating the results (recirculation length of real shape model)

Re based on the model length	2×10^5 (4m/s)	4×10^5 (8m/s)	5×10^5 (11m/s)	7×10^5 (14m/s)
Smooth flow [X/H]	1.23	1.00	1.03	1.02
Turbulent flow [X/H]	0.91	0.99	1.06	1.01

As can be seen in Figure 4.20 and 4.21, it seems that if screen is applied, then the bubble shape can be preserved well under lower Re.

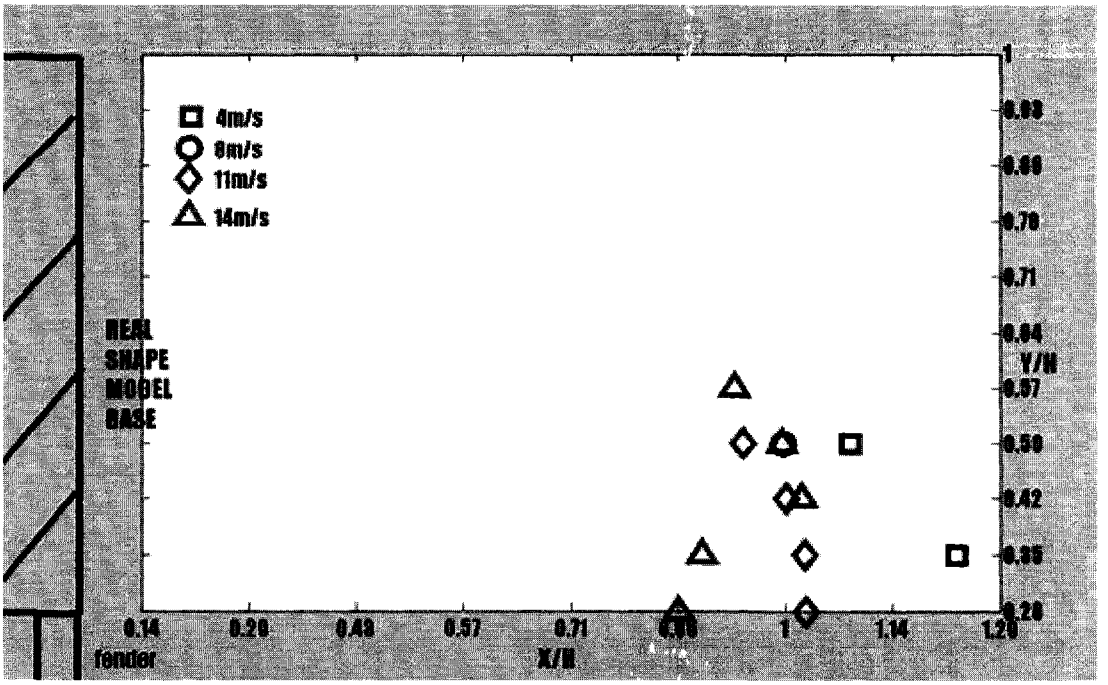

Figure 4. 20 Bubble shape under different Re,"smooth flow"

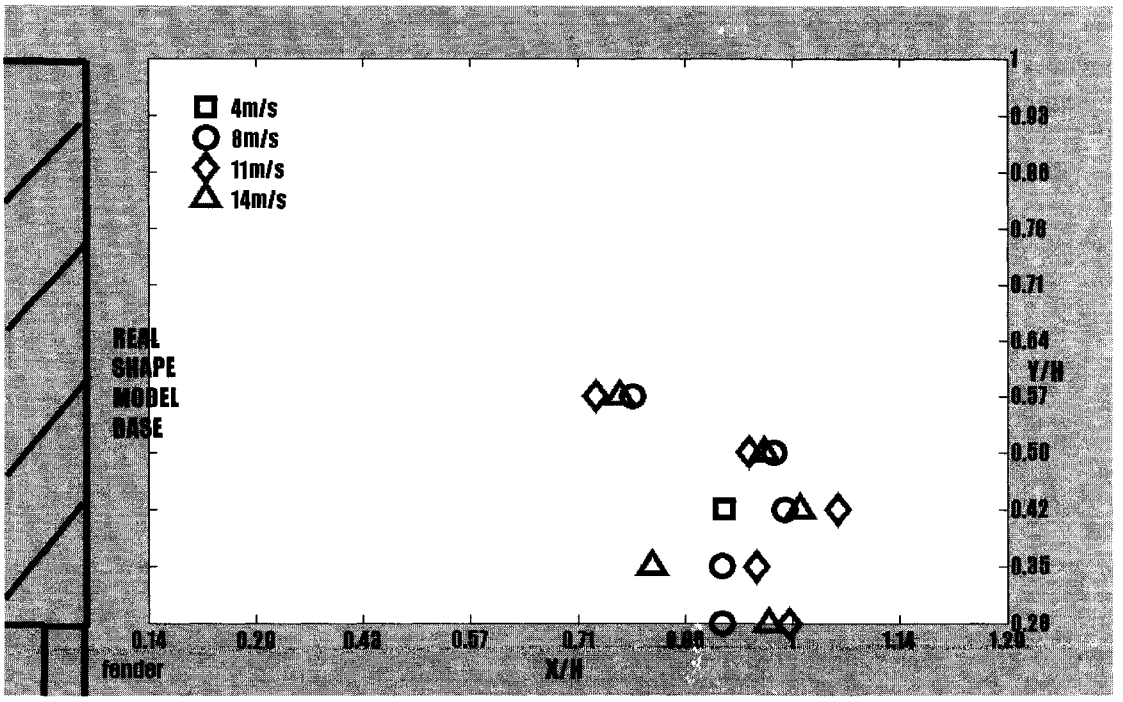

Figure 4. 21 Bbubble shape under different Re,"turbulent flow"

Figure 4.22 shows recirculation length vs. Reynolds number in a testable range for a single real shape model case.

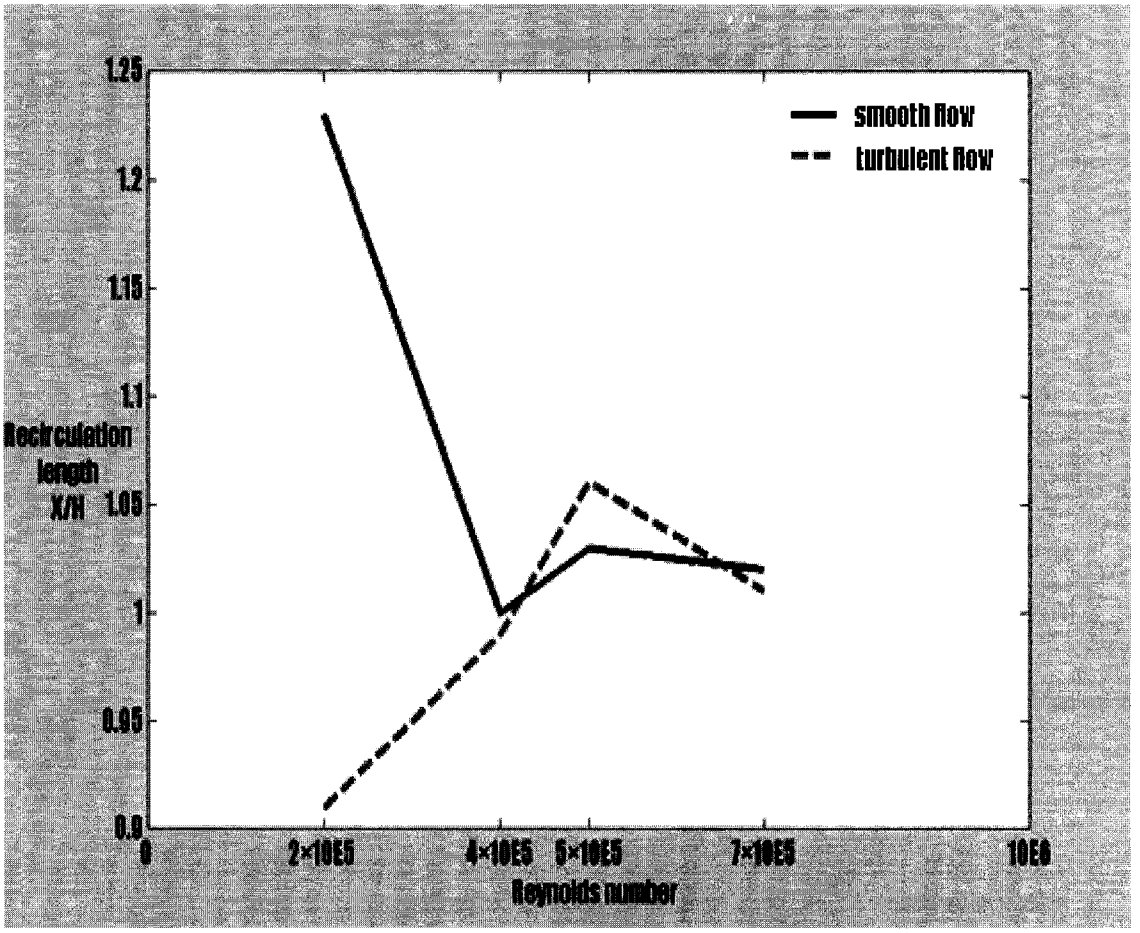

Figure 4. 22 Recirculation length vs. Reynolds number (real shape model)

All in all, taking consider both recirculation length and bubble shape, and based on Wiedeman's work in 1989, we may say that we can use $Re=4\times10^5$ with screen case (recirculation length=0.99) to extrapolate $Re=7\times10^5$ Clear flow (recirculation length =1.02).

4.6 Flow Visualization Using Tuft Grid

Since smoke is hard to handle and it is difficult to tell the bubble shape from the smoke visualization at the preliminary stage, see Figure 4.11, a tuft grid is used.

All the tuft grid visualization was done using the real shape model. See Figures 4.23-4.26 for visualization in the vertical central plane.

Figures 4.27-4.29 illustrate the transverse plane visualization, the horse shoe type of vortex occurs though it is not very clear.

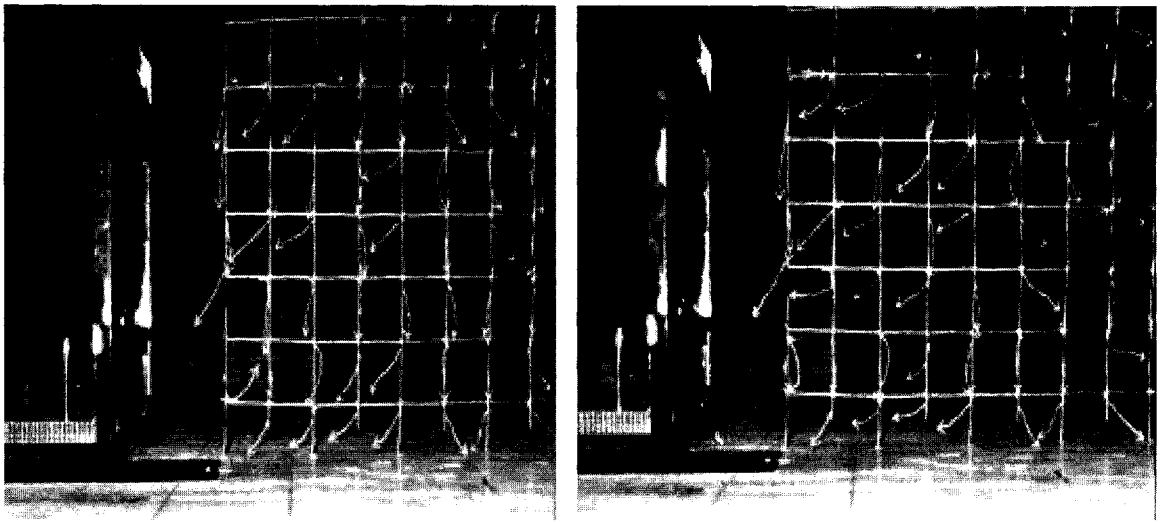

Figure 4. 23 Tuft visualization: U=4.2m/s (left) and U=8.2m/s (right)

1 inch grid size

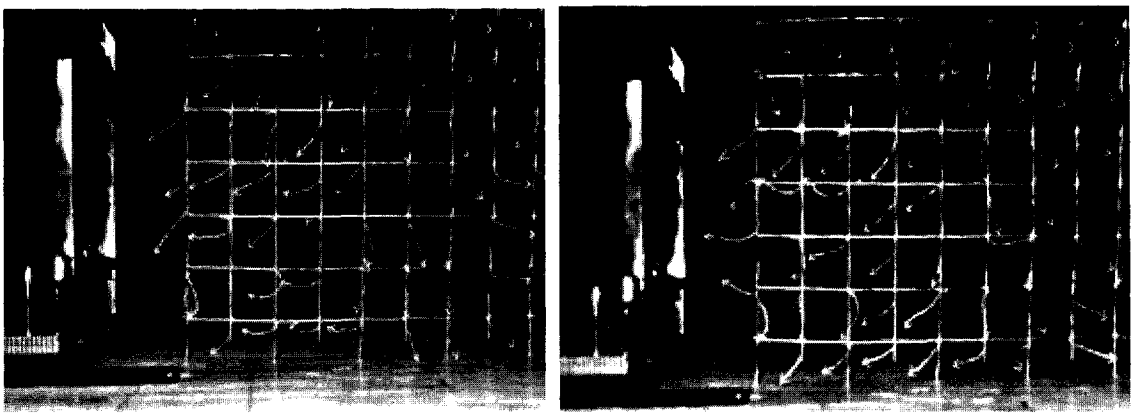

Figure 4. 24 Tuft visualization: U=11.5m/s (left) and U=14.7m/s (right)

1 inch grid size

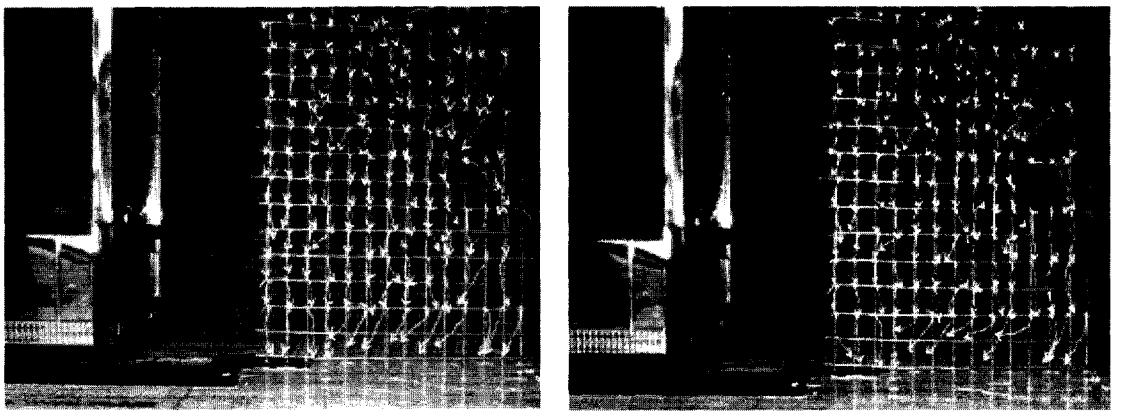

Figure 4. 25 Tuft visualization: U=4.2m/s (left) and U=8.2m/s (right)

1/3 inch grid size

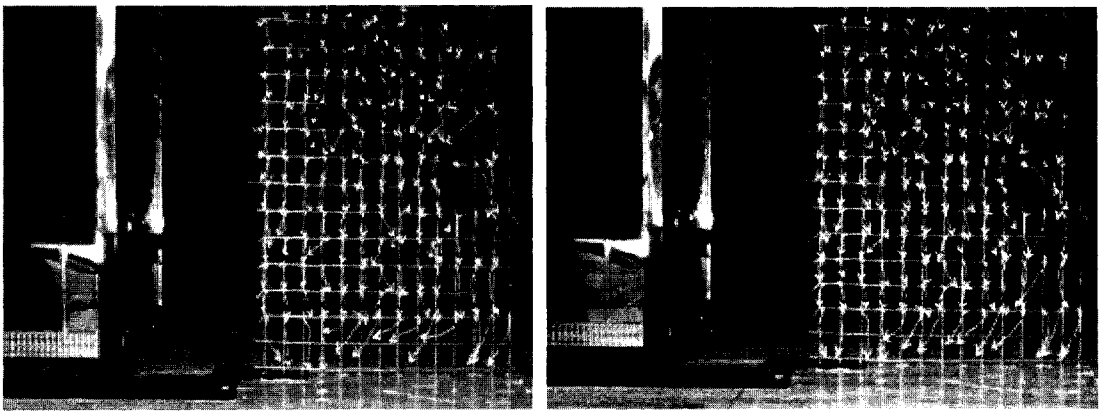

Figure 4. 26 Tuft visualization: U=11.5m/s (left) and U=14.7m/s (right)

1/3 inch grid size

Table 4.8 shows the comparison of hotwire measurement and flow visualization regarding Xr.

Table 4.8 Comparison of recirculation length of the models between two techniques (hotwire vs. tuft grid, under $Re=7\times10^5$, with elevated plate)

Model/ Recirculation length		RB	RF	GM	RS (new model with fender)
Hotwire experiment		0.66	0.78	0.65	1.02
Tuft grid visualization	1 in	0.71	0.86	0.71	1.14
	1/3 in	0.62	0.81	0.67	1

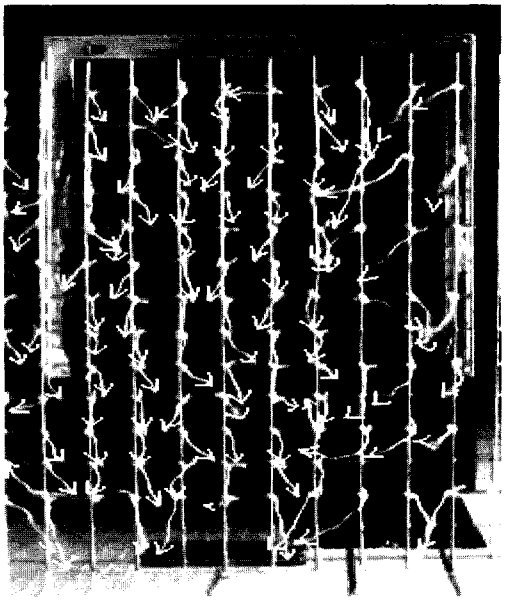

Figure 4.27 Tuft visualization: X=0.5H downstream, 14m/s freestream

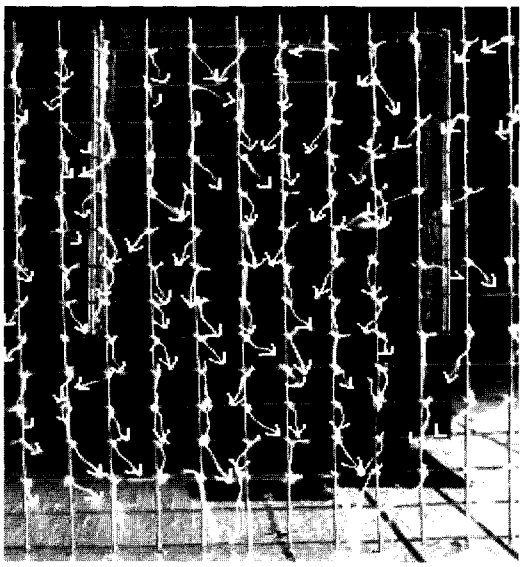

Figure 4. 28 Tuft visualization: X=H downstream, 14m/s freestream

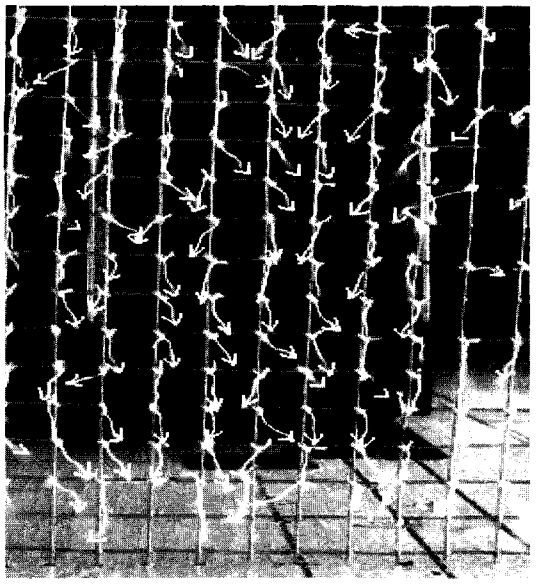

Figure 4.29 Tuft visualization: X=1.5H downstream, 14m/s freestream

There is recirculating flow in the near wake region along the vertical central planes for all the cases; the bubble shape can be detected. For the transverse planes, the well known horse shoe vortices can be found.

Chapter 5 Conclusions and Recommendations

This research was carried out to study the wake bubble of different truck models using the Dantec hotwire system. In the first series of measurement, the bubble lengths of all the truck models have been obtained. The model was placed on the wind tunnel ground board; tentative sampling number and sampling frequency were picked, the free stream was set to be around 14m/s, which is peak velocity in this research. At this stage, the shape details impact on the wake bubble is the main concern.

The elevated plate improved the ground simulation, therefore the rest of the series of measurements were all completed with the elevated plate. The tested cases are elevated plate impact, three dimensional characteristics of the wake bubble, sedan and truck in tandem arrangement as well as Re effect. At this stage, the sampling number and sampling frequency have been properly set based on the sensitivity analysis, and the free stream velocity was extended to 4m/s, 8m/s and 11m/s.

The main conclusions and recommendations are detailed as follows:

- The impact of shape details on the wake bubble is the first concern, the bubble shape of the rectangular block and that of the rounded front model are quite similar. Under the same wind conditions, the real shape model has the largest bubble length. As more model details are included, the bubble shifts

downward, towards the ground, and farther downstream. A "dual bubble" appears to occur behind the generic truck model, where the lower bubble seems to be more dominant. The upper half of the "dual bubble" has not been detected behind the most detailed truck model. In all, the shape details impact on the wake bubble is considerable.

- While the elevated plate application improved the ground simulation. The measurement regarding bubble shape of all the truck models has been repeated; it turned out there is no huge difference between the two ground simulations though generally the latter one is expected to be better.

- After the application of elevated plate, the side planes are investigated in order to find out the three dimensional characteristics of the bubble in the near wake of all the four truck models. The result showed that the rounded front model has the largest bubble region while the other three are almost identical.

- The sedan and truck in tandem case is also studied, the impact of leading sedan on the wake of truck is investigated. The bubble shrinks at the central plane (z=0) and extends at the side plane ($z=\pm w/8$) as the spacing between the leading sedan and truck decreases. Furthermore, the scope of the bubble does not change because of the presence of the leading sedan.

- The Reynolds number covered in this study is similar to that obtained by Duell and George [1993, 1999]; Re = 7×10^5 corresponds to 2.1 km/h in the real scenario. Based on Wiedeman's work in 1989, we found that we may say that we can use Re=4×10^5 with screen case (recirculation length=0.99) to extrapolate Re=7×10^5 Clear flow (recirculation length =1.02), which means the effective Reynolds number can be increased by turbulence manipulation; While whether the current results is valid or not is unknown for higher Reynolds number. In other words, the future work needs to be extended to higher Reynolds numbers to ensure the results obtained in these low Reynolds number studies are valid in real life.

- Flow visualization is also conducted in order to support the current hotwire results. Since the smoke is hard to handle, our focus is on the tuft grid visualization, the recirculating flow in the near wake region along the vertical central planes can be visualized; the bubble shape can also be detected. For the transverse planes, the well known horse shoes can be found although it is not obvious.

- The wake bubble of the road vehicle can be treated as part of the body as far as aerodynamics is concerned. If the "whole body" is getting more streamlined, the drag may be reduced which will lead to improved fuel economy. Drag measurements need to be done in the future to validate this point.

References

1. M. Ahmadi and K. P. Garry, Preliminary Investigation of the Influence of a Ground-Plane Boundary Layer on the Aerodynamics Characteristics of Road Vehicle Models Tested Over a Fixed Ground, SAE 960675, 1996

2. S. R. Ahmed, G. Ramm and G. Faltin, "Some salient features of the time-averaged ground vehicle wake", SAE paper 840300, 1984

3. J. W. Allan, "Aerodynamic drag and pressure measurements on a simplified tractor-trailer model", Journal of Wind Engineering and Industrial Aerodynamics, v9, p 125-136, 1981

4. A. F. Azim, "An experimental study of the aerodynamic interference between road vehicles", SAE paper 940422, 1994

5. J. B. Barlow, W. H. Rae, Jr. Alan Pope, "Low-speed wind tunnel testing", Third edition, Wiley Interscience, 1999

6. E. G. Duell, A. R. George, "Measurements in the unsteady near wake of ground vehicle bodies", SAE paper 930298, 1993

7. E. G. Duell, A. R. George, "Experimental study of a ground vehicle body unsteady near wake", SAE paper 990812, 1999

8. Abdullah M. Al Garni, Fundamental investigation of road vehicle aerodynamics, PHD dissertation, University of Michigan, 2003

9. Kevin P. Garry, Wind tunnel tests on the influence of fixed ground board length on the aerodynamic characteristics of simple commercial vehicle models, Journal of Wind Engineering and Industrial Aerodynamics, v38, n1, p 1-10, 1991

10. Robert A. Granger, Fluid Mechanics, CBS college publishing, 1985

11. Donald S. Gross and William S. Seksecienski, Some problems concerning wind tunnel testing of automotive vehicles, SAE 660385, 1966

12. M. Hammache, M. Michaelian, F. Browand, "Aerodynamic Forces on Truck Models, Including Two Trucks in Tandem", Research Report UCB.ITS.PRR.2001.27, 2001

13. W.H. Hucho, "Aerodynamics of road vehicles", Annu. Rev. Fluid Mech, v25, p 485-537, 1993

14. W. H. Hucho (Ed.), "Aerodynamics of road vehicle: From fluid mechanics to vehicle engineering", Fourth edition, SAE International, 1998

15. Finn E. Jorgensen, How to measure turbulence with hot-wire anemometers- a practical guide, Dantec Dynamic, 2002

16. Hermann Lienhart and Stefan Becker, Flow and Turbulence Structure in the Wake of a Simplified Car Model, SAE 2003-01-0656, 2003

17. V. Losito and C.de Nicola, An improved method of computing the wake effects on aerodynamic characteristics of road vehicle, International Journal of Vehicle Design, special publication sp3, 1983

18. R. J. Martinuzzi, B. Havel, "Vortex shedding from two surface-mounted cubes in tandem", International Journal of Heat and Fluid Flow, v25, p 364-372, 2004

19. R. McCallen, "Working group meeting on heavy vehicle aerodynamic drag", UCRL-ID-133547, 1999

20. T. Morel, The effect of base slant on the flow pattern and drag of three-dimensional bodies with blunt ends, AIChE Symposium Serises, p 191-226, 1978

21. C.T. Shaw, K.P. Garry, T. Gress, "Using singular systems analysis to characterize the flow in the wake of a model passenger vehicle", Journal of Wind Engineering and Industrial Aerodynamics 85 (2000) 1-30

22. K. Sinisa, "Large-eddy simulations for computing the flow around vehicles", Doktorsavhandlingar vid Chalmers Tekniska Hogskola, n 1870, p 1-55, 2002

23. M. Sitlani, K. Aung, "Numerical simulations on the aerodynamics drag of a tractor with a tandem-trailer", 2006 ASME joint U.S. – European Fluids Engineering Summer Meeting, FEDSM 2006

24. Hubert Smith, the illustrated guide to aerodynamics. 2ND Edition, 1992

25. J. Wiedemann, Turbulence manipulation to increase effective Reynolds numbers

in vehicle aerodynamics, v27, AIAA journal, p 763-769, 1989

26. J. J. Villanueva, Visualization, imaging, and image processing, Proceedings of the Second IASTED International Conference in USA, 2002

27.http://www.autobytel.com/content/shared/articles/templates/index.cfm/article_id_int/1188, accessed September 25, 2007

28. External flows: Bluff Bodies, Mechanical Engineering notes, SESM2007-FLUID MECHANICS

29. G. N. V. Rao, Extrapolation of wind tunnel model results to full scale, wind loads on structures, 1990

Appendix A. Calculation of displacement thickness (wind tunnel board)

Empty test section, locates at the rear of truck model

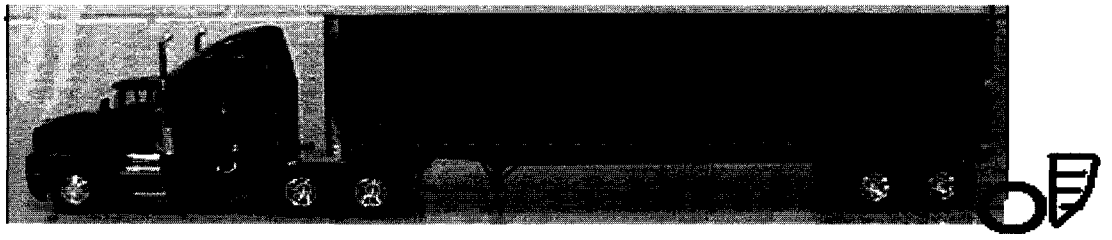

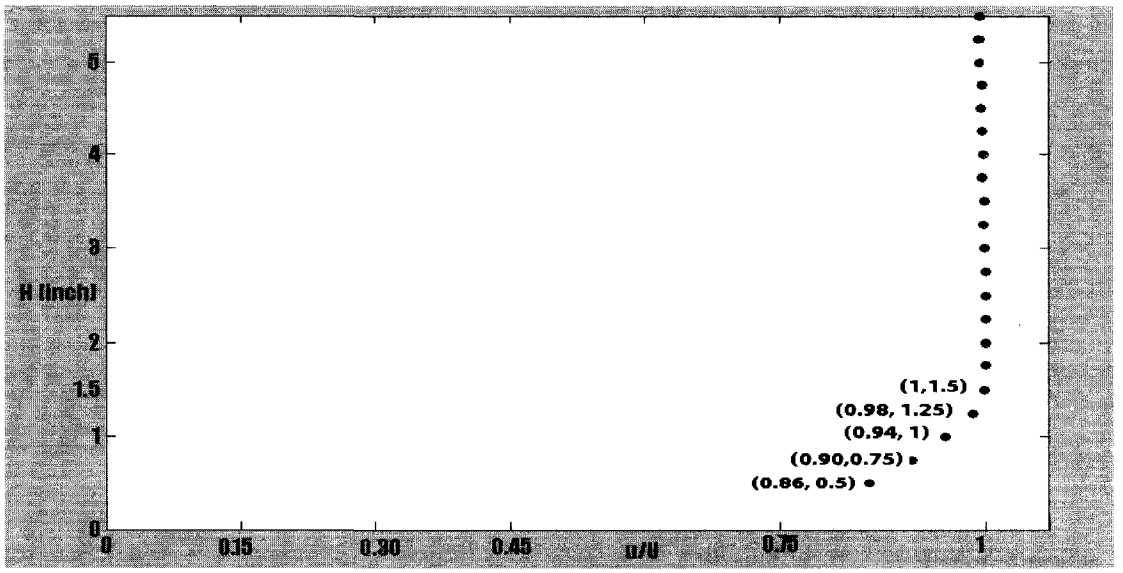

Figure A.1 Measurement of boundary layer

$$\delta^* = \int_0^{\delta} \left(1 - \frac{u}{U}\right) dy$$

$where \delta = 1.5inch = 0.04\text{m}$

$$\delta^* = \int_0^{0.5\delta} \left(1 - \frac{u}{U}\right) dy + \int_{0.5}^{1.5\delta} \left(1 - \frac{u}{U}\right) dy = 0.5 \times (1 - 0.86) + 0.25 \times [(1 - 0.9) + (1 - 0.94) + (1 - 0.98)] = 0.115 \quad \text{inch}$$

Thus, displacement thickness/ground clearance of the truck model=0.115/1.968=6%<10%, thus the effect of fixed tunnel board is expected to be small.

Appendix B. Uncertainty of a velocity sample

A: old calibration system: coupled with pitot tube
(Raw data of $U_{sample1}$=10.9m/s)
B: New calibration system: auto-calibrator
(Raw data of $U_{sample2}$= 13.4m/s， $U_{sample3}$= 3.3m/s)
Table A.1

Source of uncertainty	Input variants		Typical value ΔX_i	Relative output varians	Typical value $\Delta Y_i/U$	Coverage factor K	Relative standard uncertainty $\Delta Y_i/kU$
Calibration	A $U_{sample1}$	ΔU_{cal}	2%	2STDV(100 ΔU_{cal})	0.04	2	0.02
	B $U_{sample2,3}$		1%, 1.6%①		0.02, 0.032		0.01, 0.016
Linearization	A $U_{sample1}$	ΔU_{fit}	0.485%	2STDV(100 ΔU_{fit})	0.0097	2	0.00485
	B $U_{sample2,3}$		0.340%		0.0068		0.00340
A/D resolution	E_{AD}		10 volts	$\frac{1}{U}\frac{E_{AD}}{2^n}\frac{\partial U}{\partial E}$	0.009	$\sqrt{3}$	0.005
	n		12 bit		0.009, 0.014②		0.005, 0.008
Relative expanded uncertainty	$U(U_{sample}) = 2\sqrt{(\Delta y_i / kU)^2}$ U1 =0.042=4.2% U2=0.023=2.3% U3=0.036=3.6% ③						

The other factors such as ambient pressure, humidity are neglected because of the relative small standard uncertainty.
When the uncertainty of calibration equipment is included, the uncertainty of velocity sample 1 and 2 are 4.2% and 2.3% respectively.
Thus

$U_{sample1}$=10.9±0.5m/s
$U_{sample2}$=13.4±0.3m/s
$U_{sample3}$= 3.3±0.1m/s

Note:

① STDV($U_{calibrator}$) =±a (%)+b(m/s)

	a (%)	b (m/s) when U<5m/s
auto calibrator	±1	±0.02
calibration with pitot-static tube	±2	N/A

Sample calculation under the velocity of 3.3m/s:
Since U<5m/s,
STDV($U_{calibrator}$) =±a (%)+b(m/s)= ±1%±0.02=±1%±(0.02/3.3*100)%= ±1.6%

② Calculation of $\frac{1}{U}\frac{E_{AD}}{2^n}\frac{\partial U}{\partial E}$ under the velocity sample of 3.3m/s:

U=3.3m/s, E_{AD}=10volts, n=12bit,
$U=c0+c1\times E+c2\times E^2+c3\times E^3+c4\times E^4$,
Where,
c0=-80.452705;
c1=169.321381;
c2=-121.294373;
c3=29.509886;
c4=0.000009;

Thus $\left.\frac{\partial U}{\partial E}\right|_{U=3.3}$ =18.8 m/s/volt

So, $\frac{1}{U}\frac{E_{AD}}{2^n}\frac{\partial U}{\partial E}$ =0.014

③ From the manual of dantecdynamcis, uncertainty calculation of a 15m/s velocity sample (auto calibrator) is 3%.

Reference;
Finn E. Jorgensen, How to measure turbulence with hot-wire anemometers- a practical guide, dantec dynamic literature, 2002

Appendix C. Sensitivity analysis

Sampling number:

Sampling number of previous work is set to be large (2^{21}=2,097,152):

In real shape truck model case, grid point of minimum local mean velocity has been chosen as a sample for sampling number sensitivity analysis, as can be seen below:

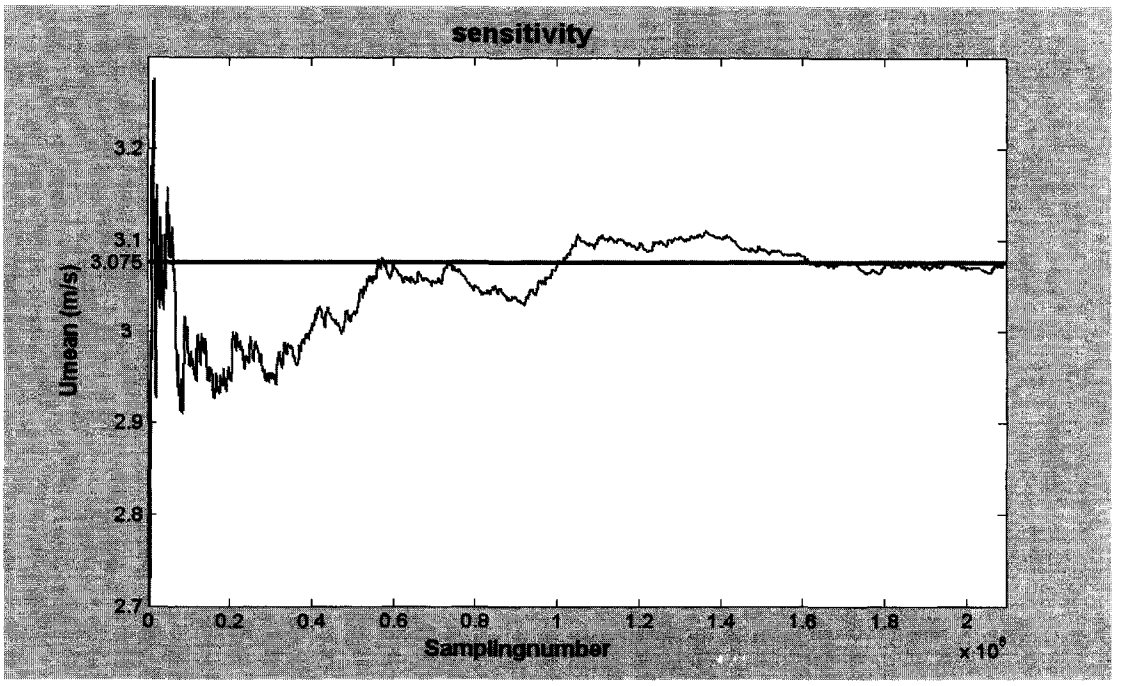

Figure B.1 mean velocity vs. sampling number (x=1:1: sampling number)

It seems after 1.6×10^6, the time averaged velocity tends to be uniform.

The other three cases have been checked out, and measured grid points were picked randomly. Here are some samples:

Generic truck model case

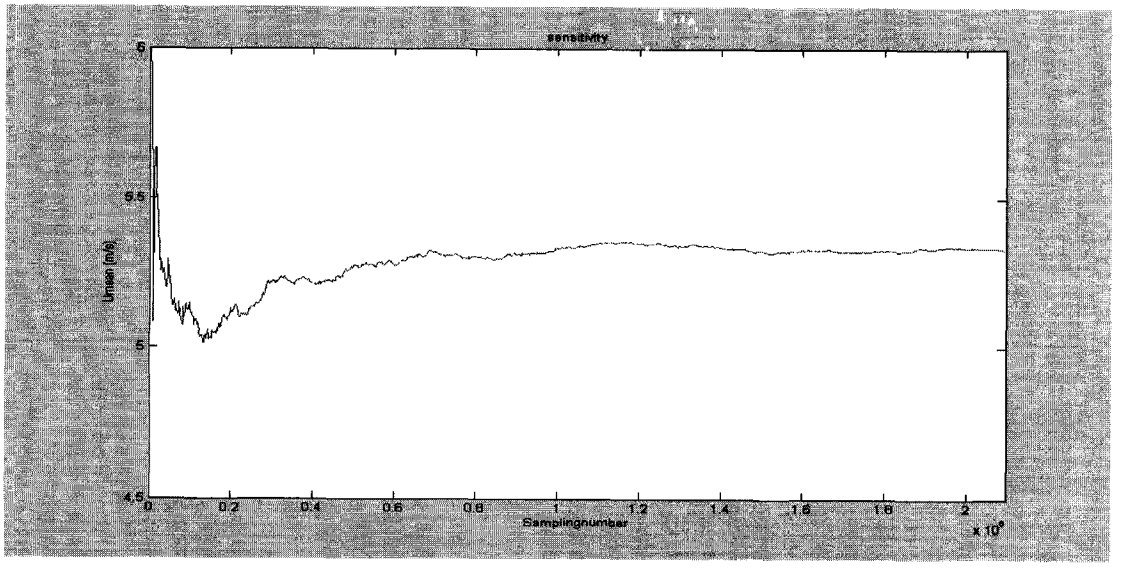

Figure B.2 mean velocity vs. sampling number (x=1:2048: sampling number)

Rounded front truck model case

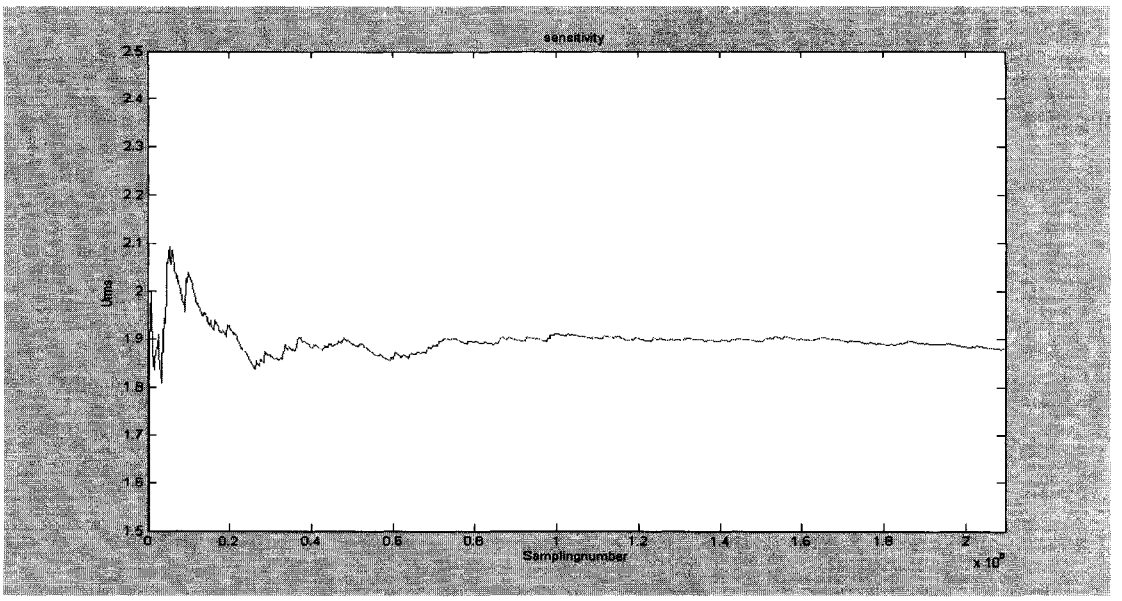

Figure B.3 mean velocity vs. sampling number (x=1:2048: sampling number)

Rectangular block model case

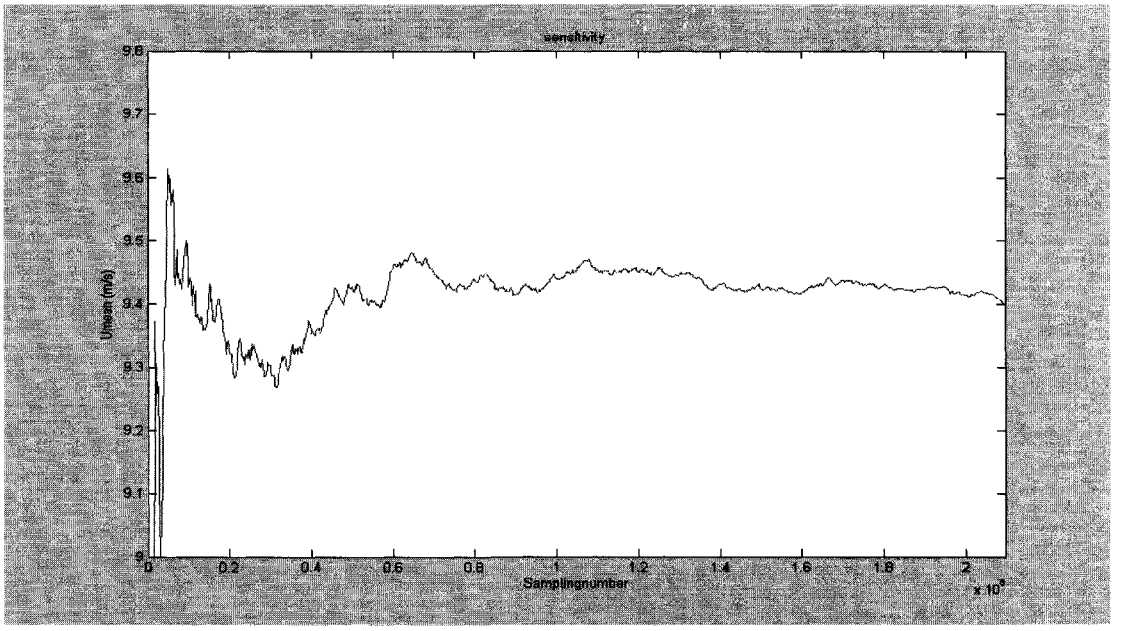

Figure B.4 mean velocity vs. sampling number (x=1:2048: sampling number)

To sum up, at the sampling frequency of 75kHz, freestream velocity of 14m/s, the proper sampling number of the data is around 1.6×10^6

Sampling frequency:

Sampling frequency (75kHz)

The sampling rate is determined by the maximum frequency component in the flow.

In order to meet Nyquist–Shannon sampling theorem, the sampling frequency has been chosen as $2 \times f_{cutting}$ or $2.5 \times f_{cutting}$, this cutting frequency can be obtained in the "square wave test" during calibration. The square wave test is conducted under the potential maximum velocity of the measurement. For our case, the maximum velocity is around 20m/s, and the corresponding cutting frequency is around 30kHz, theoretically, the sampling frequency should be 60 or 75kHz.

In order to validate this sampling frequency, two sets of velocity data have been collected under the condition of freestream velocity of 14m/s and sampling number of 1.6×10^6

Case1: free stream of around 14 m/s

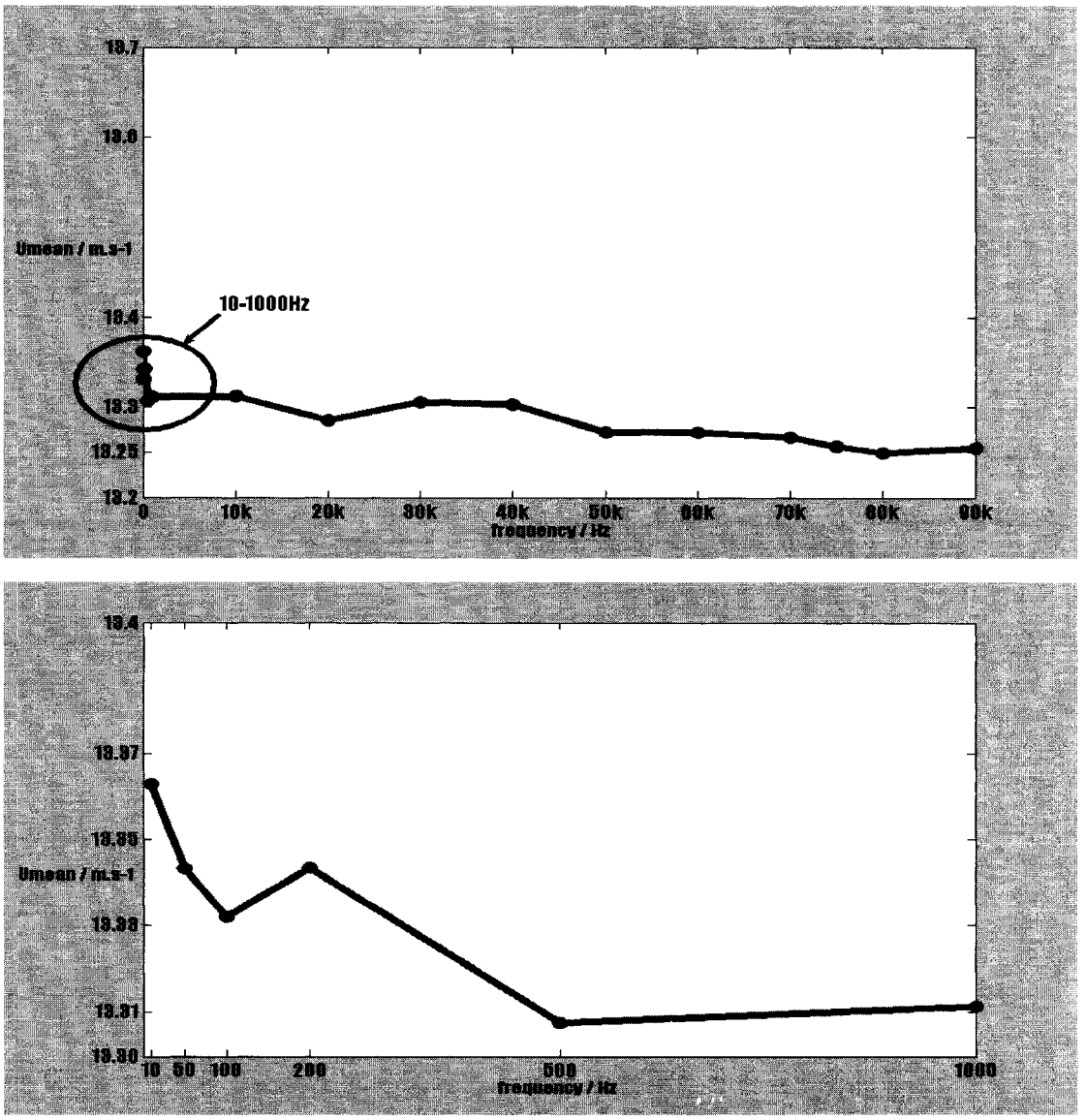

Figure B.5 Umean vs. sampling frequency

The time averaged velocity finally converges to 13.25 m/s.

Case2: sample point behind model under around 14 m/s freestream velocity

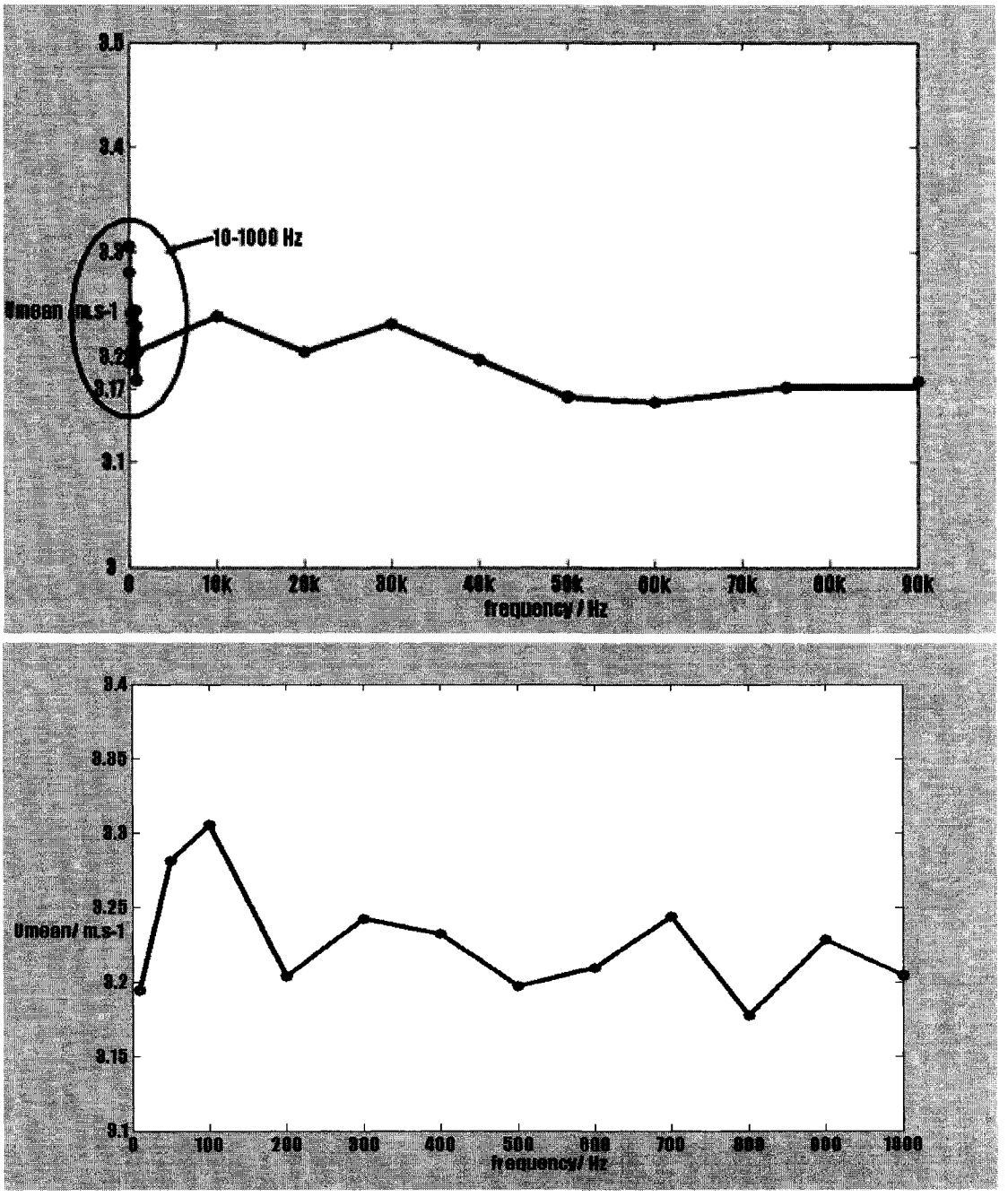

Figure B.6 Umean vs. sampling frequency

The time averaged velocity finally converges to 3.17 m/s.

From the figures above, we can draw a conclusion that the sampling frequency 75 kHz is adequate in the series of measurements.

Appendix D. Traverse program (motion control of the transverse system)

Program 1_ vertical motion

```
RUN?
UAI
UBO
hh=11
%% The traversing in the VERTICAL direction will repeat 16 times
vv=10
%% The traversing will move VERTIVALLY FOR TOTAL-1 times at each HORIZONTAL position
a=1
b=1
O=0
PRINT("VERT1_VERTICAL POSITION")
RP
A=100
V=500000
WHILE a<=hh
C10 WHILE b<=vv
c=UAI
WHILE c==1
UB=1
c=UAI
LOOP
O=0
PRINT("VERT2_VERTICAL POSITION RIGHT BEFORE MOVE")
RP
D=-5000
G
TWAIT
WAIT=10000
UB=0
b=b+1
GOTO10
LOOP
c=UAI
```

```
WHILE c==1
UB=1
c=UAI
LOOP
b=b-1
O=0
PRINT("VERT3_VERTICAL POSITION")
RP
D=5000*b
G
TWAIT
WAIT=20000
UB=0
a=a+1
b=1
LOOP
PRINT("VERT4_PROGRAM VERTICAL ENDS")
END
```

Program 2_ horizontal motion

```
RUN?
UAI
UBO
b=1
hh=10
%% The traversing mechanism will 10 (TOTAL-1) times in the HORIZONTAL direction.
A=100
V=500000
C10 WHILE b<=hh
c=UAI
WHILE c==1
UB=1
c=UAI
LOOP
PRINT("HORZ1_MOVE HORIZONTALLY ONCE")
D=5000
G
```

```
TWAIT
WAIT=20000
UB=0
b=b+1
GOTO10
LOOP
PRINT("HORZ2_HORIZONTAL PROGRAM ENDS")
END
```

Appendix E. Data collection program

C program code for DMA_XFER_1D.exe

```
#include <fstream.h>
#include <stdio.h>
#include <assert.h>
#include <windows.h>
#include "C:/nidaq/nidaq.h"
#include "C:/nidaq/nidaqcns.h"

short status;
const short port=0, deviceNumber=1, dir_in=0, dir_out=1, line_A_1=0, line_B_1=1,
line_A_2=2,line_B_2=3;
const ready=0,not_ready=1;
short *state_MH = new short,*state_MV = new short;

int Collect_Data_2d(char* binary_indicator, double SampleRate, unsigned long
SampleNumber, short inputMode, char *folderName, int zone, int count_Horizontal,
int count_Vertical);
void Collect_Data_1d(double SampleRate, unsigned long SampleNumber, short
inputMode,char *folderName,int zone,int count_Horizontal,int count_Vertical);
char* get_filename (char* folderName, int zone, int count_Horizontal, int
count_Vertical);
void Save_Data_2d(char* binary_indicator,unsigned long count, short* buffer, char*
filename,short *reading);
void Save_Data_1d(unsigned long count, short* buffer, char* filename,short
*reading);
int main()
{
    cout<<"No. of point in the vertical direction:";
    int vertical_limit;
    cin>>vertical_limit;
    cout<<"No. of point in the horizontal direction:";
    int horizontal_limit;
    cin>>horizontal_limit;

    //The folreadying sets the communication lines 0,1,2,3.
```

```
cout<<"\nSample Rate (Hz): ";
double SampleRate;
cin>>SampleRate;
cout<<"\nSample Number: ";
unsigned long SampleNumber;
cin>>SampleNumber;
cout<<"\nZone No.: ";
int zone;
cin>>zone;
cout<<"\nFolder Name: ";
char *folderName = new char[80];
cin>>folderName;
cout<<"\nInput MODE (0 diff 1 RSE 2 NRSE): ";
short inputMode;
cin>>inputMode;
cout<<"\nSave data in binary format(Y or N): ";
char *binary_indicator = new char;
cin>>binary_indicator;

    //This output is WRT the daq board->motor
status = DIG_Line_Config(deviceNumber, port, line_A_1, dir_out);
assert(status==0);

    //make sure there is no horizontal traversing
    status=DIG_Out_Line(1, 0, 0, 1);
assert(status==0);

    //This input is WRT the daq board->motor
status = DIG_Line_Config(1, 0, 1, 0);
assert(status==0);

    //This output is WRT the daq board->motor
status = DIG_Line_Config(1, 0, 2, 1);
assert(status==0);


    //make sure there is no horizontal traversing
status=DIG_Out_Line(1, 0, 2 1);
assert(status==0);

    //This input is WRT the daq board->motor
```

```
    status = DIG_Line_Config(1,0,3,0);
    assert(status==0);

    //Preparation is done, real work starts from here
    for(int count_Horizontal = 1; count_Horizontal<=horizontal_limit;
count_Horizontal++)
    {
        for (int count_Vertical=1; count_Vertical<=vertical_limit; count_Vertical++)
        {
            printf("\n%d    %d",count_Horizontal,count_Vertical);


                        Collect_Data_1d(SampleRate, SampleNumber,
                        inputMode, folderName, zone, count_Horizontal,
                        count_Vertical);

            //activate the traversing, move to next position
            status=DIG_Out_Line(1,0,0,0);
            assert(status==0);

                    //get the status of the traversing, move done or not?
            status=DIG_In_Line(1,0,1,state_MV);
            assert(status==0);

            //Test whether or not the probe is in position
            while (*state_MV==1)
            {
                status=DIG_In_Line(1,0,1 ,state_MV);
                assert(status==0);
            }//move is done,start new data collection

                    //make sure does not traverse vertically
            status=DIG_Out_Line(1,0,0,1);
            assert(status==0);
        }//traversing will return to its vertical origin, since line_A_1 is ready.
            //at this poit, the port A_1 is in ready status, port B_1 is at 0 (READY
          FOR DATA //COLLECTION) status.

          //it's time to make a horizontal traversing

          //activate the traversing, move to next position
```

```
        status=DIG_Out_Line(1,0,2,0);
        assert(status==0);

            //get the status of the traversing, move done or not?
        status=DIG_In_Line(1,0,3,state_MH);
        assert(status==0);

            //Horizontal traversing should be done at this point. The H motor
            should send back a //ready signal

        //Test whether or not the probe is in position
        while (*state_MH==1)
        {
            status=DIG_In_Line(1,0,3,state_MH);
            assert(status==0);
        }//move is done,start new data collection

            //activate the traversing, move to next position
        status=DIG_Out_Line(1,0,2,1);
        assert(status==0);
    }
    return 1;
}

char* get_filename (char* folderName, int zone, int count_Horizontal, int
count_Vertical)
{
    char *filename_return = new char[40];
    strcpy(filename_return,folderName);
    char pZONEc[1];
    char pZEROHc[1];
    char pZEROVc[1];

    char pCOUNT_HORIZONTALc[2];
    char pCOUNT_VERTICALc[2];

    if (count_Horizontal < 10)
    {
        _itoa(0,pCOUNT_HORIZONTALc,10);
        _itoa(count_Horizontal,pZEROHc,10);
        strcat(pCOUNT_HORIZONTALc,pZEROHc);
```

```
    }
    else
        _itoa(count_Horizontal,pCOUNT_HORIZONTALc,10);

    if (count_Vertical < 10)
    {
        _itoa(0, pCOUNT_VERTICALc,10);
        _itoa(count_Vertical, pZEROVc,10);
        strcat(pCOUNT_VERTICALc,pZEROVc);
    }
    else
        _itoa(count_Vertical,pCOUNT_VERTICALc,10);

    _itoa(zone,pZONEc,10);
    char *pDotTxt = ".txt";

    strcat(filename_return,pZONEc);
    strcat(filename_return,pCOUNT_HORIZONTALc);
    strcat(filename_return,pCOUNT_VERTICALc);
    strcat(filename_return,pDotTxt);

    pDotTxt = NULL;

    return filename_return;
}

void Collect_Data_1d(double sampleRate, unsigned long SampleNumber, short
inputMode, char *folderName, int zone, int count_Horizontal, int count_Vertical)
{
    short status, deviceNumber=1, chan0=0, chan1=1, gain = 1, inputRange = 10,
polarity=1, driveAIS = 1;
    unsigned long count = SampleNumber;
    short *buffer = new short[count];
    char *filename = new char[40];
    short *reading = new short[1];
    filename = get_filename (folderName, zone, count_Horizontal, count_Vertical);

    printf("\nPlease wait, data is being collected");
    status = AI_Configure (deviceNumber, chan0, inputMode, inputRange, polarity,
driveAIS);
    assert(status==0);
```

```
    status = AI_Configure (deviceNumber, chan1, inputMode, inputRange, polarity,
driveAIS);
    assert(status==0);

    status = DAQ_Op (deviceNumber, chan0, gain, buffer, count, sampleRate);
    printf("%d",status);
    assert(status==0);
    status = AI_Read (deviceNumber, chan1, gain, reading);
    assert(status==0);
    Save_Data_1d(count, buffer, filename, reading);

    printf("\nGo");
}
void Save_Data_1d(unsigned long count, short* buffer, char* filename,short
*reading)
{
    printf("\nSaving data to disk.");

    ofstream fout(filename, ios::app);

    for(unsigned long count_data = 0; count_data<count;count_data++)
    {
        fout<<"\n"<<*(buffer+count_data);
    }
    fout<<"\n"<<*reading;
    fout.close();
    printf("\nSavind data completed");
```

Vita Auctoris

Dongqing Yang was born in 1982 in Datong, Shanxi, P. R. China. He obtained his Bachelor of Engineering at Beijing Institute of Technology in 2005. Currently he is a candidate for the Master's degree in Mechanical Engineering at the University of Windsor and hopes to graduate in Summer 2008.